AGU PUBLICATIONS

Geochemistry, Geophysics, Geosystems

RESEARCH ARTICLE
10.1002/2016GC006712

Large-volume lateral magma transport from the Mull volcano: An insight to magma chamber processes

Osamu Ishizuka[1,2], Rex N. Taylor[3], Nobuo Geshi[1], and Nobutatsu Mochizuki[4]

[1]Research Institute of Earthquake and Volcano Geology, Geological Survey of Japan, AIST, Tsukuba, Japan, [2]Japan Agency for Marine-Earth Science and Technology, Yokosuka, Japan, [3]Ocean and Earth Science, University of Southampton, National Oceanography Centre, European Way, Southampton, [4]Priority Organization for Innovation and Excellence, Kumamoto University, Kumamoto, Japan

Key Points:
- The magma flow direction within dikes from the Mull volcano gradually changed from near vertical to horizontal within 30 km of its center
- Magma assimilating lower crust only forms proximal dikes and feeds overlying upper crustal reservoir which forms proximal or distal dikes
- Magma volumes from basaltic lower and felsic upper crustal reservoirs were combined to generate andesitic long-distance dikes

Supporting Information:
- Supporting Information S1
- Table S1
- Table S2
- Table S3

Correspondence to:
O. Ishizuka,
o-ishizuka@aist.go.jp

Citation:
Ishizuka, O., R. N. Taylor, N. Geshi, and N. Mochizuki (2017), Large-volume lateral magma transport from the Mull volcano: An insight to magma chamber processes, *Geochem. Geophys. Geosyst.*, *18*, 1618–1640, doi:10.1002/2016GC006712.

Received 2 NOV 2016
Accepted 30 MAR 2017
Accepted article online 12 APR 2017
Published online 19 APR 2017

Abstract Long-distance lateral magma transport within the crust has been inferred for various magmatic systems including oceanic island volcanoes, mid-oceanic ridges, and large igneous provinces. However, studying the physical and chemical properties of active fissure systems is difficult. Hence, this study investigates the movement of magma away from the Mull volcano in the North Atlantic Igneous Province, where erosion has exposed its upper crustal dike networks. Magmatic lineations within dikes indicate that the magma flow in the Mull dike suite changed from near vertical to horizontal within 30 km of the volcanic center. This implies that distal dikes were fed by lateral magma transport from Mull. Geochemical characteristics indicate that many $<$50 km long dikes have deep crustal signatures, reflecting storage and assimilation in Lewisian basement. Following crystallization and assimilation in the lower crust, magma fed an upper crustal reservoir, where further fractionation and incorporation of Moinian rocks generated felsic compositions. Distal dikes are andesitic and reflect events in which large volumes of mafic and felsic magma were combined by mixing between lower and upper crustal reservoirs to generate the 30–80 km^3 required to supply the long-distance dikes. Once propagated, compositions along dikes were not significantly affected by assimilation and crystallization. Supplying the distal dikes with magma would have required a large-scale evacuation of the crustal reservoirs that acted as a potential trigger for explosive volcanism and the caldera formation recorded in Mull central complex.

1. Introduction

Long-distance magma transport within the Earth's crust is an important process that shapes the structure of volcanic edifices and is a significant, yet unseen, contributor to crustal growth. This lateral transport has been recognized in various volcanic settings including large igneous provinces [e.g., *Ernst and Buchan*, 1997; *Magee et al*., 2012a, 2012b, 2016], hot spot volcanoes [e.g., *Ryan*, 1988; *Klugel et al*., 2015], mid-oceanic ridges [*Dziak et al*., 1995; *Sinton et al*., 2002], and island arc volcanoes [e.g., *Hildreth and Fierstein*, 2000; *Geshi et al*., 2002; *Ishizuka et al*., 2008, 2014, 2015]. There is increasing evidence from active volcanic systems for lateral magma movement based on the migration of seismic swarms [e.g., *Einarsson and Brandsdottir*, 1980; *Toda et al*., 2002; *Peltier et al*., 2005; *Aloisi et al*., 2006], ground deformation [e.g., *Nishimura et al*., 2001; *Aloisi et al*., 2006; *Peltier et al*., 2008], emanation of volcanic gases [e.g., *González et al*., 2013], and the formation of eruption fissures [e.g., *Nakamura*, 1977]. Major factors controlling lateral transport seem to be the regional and local crustal stresses [e.g., *Watanabe et al*., 1999; *Pinel and Jaupart*, 2004] combined with the magma overpressure and physical properties (e.g., density and viscosity) of the magma and country rocks [e.g., *Rubin*, 1990; *Lister and Kerr*, 1991]. Numerical modeling predicts that the magma composition as well as the distance and direction of transport can vary depending on the shape, size, and depth of the source magma chamber as well as the size and aspect of the volcanic edifice [e.g., *Pinel and Jaupart*, 2004].

Active oceanic island volcanoes such as Kilauea provide detailed information about magma movement and its controlling factors. Based on seismic and geodectic data at Kilauea volcano, lateral magma injection occurs from reservoirs at 1 and 3 km beneath the surface [*Poland et al*., 2014]. This dike intrusion at Kilauea is triggered by both an increase in magma pressure within a magma reservoir and extensional stress [e.g., *Owen et al*., 2000]. An eruption and intrusion started on 17 June 2007 was an example of dike formation in which both magma pressure and extensional stress contributed to the lateral injection [*Poland et al*., 2008].

Martí et al. [2013] demonstrated that lateral magma transport from an eruption of El Hierro volcano in the Canary Islands was controlled by the local stress field. In this case, a flexural effect generated by the island's mass, as well as the prevailing tectonic stress, facilitated the lateral migration of magma along the crust/mantle discontinuity.

Spreading and rifting environments, such as Iceland and Afar, also provide examples of active lateral magma transport [e.g., *Einarsson and Brandsdottir*, 1980; *Ebinger and Casey*, 2001]. In the Krafla 1975–1984 rifting episode, seismic data indicated that magma laterally migrated at velocities of ~1–2 km/h away from a single crustal magma reservoir located at the center of the segment [e.g., *Tryggvason*, 1984; *Björnsson*, 1985]. InSAR measurement between August 1999 and April 2000 at Eyjafjallajökull volcano revealed that magma migrated horizontally southward, producing inflation on the southern flank of this volcano before a cessation of the unrest [*Pedersen and Sigmundsson*, 2006]. In 2014–2015, Bárdarbunga volcano provided a spectacular example of lateral magma transport from a magma reservoir that triggered caldera collapse [*Gudmundsson et al*., 2016]. A caldera area of 110 km^2 was formed, while magma drained laterally for 48 km and erupted as a major lava flow [*Gudmundsson et al*., 2016]. In Afar, seismic data indicated that velocities of lateral dike migration are in the same range as Krafla or those deduced for slow spreading mid-oceanic ridges [~1–2 km/h) [*Grandin et al*., 2011]. In terms of the driving force for lateral dike propagation, *Grandin et al*. [2012] proposed that a horizontal pressure gradient along the slope of the brittle-ductile transition zone beneath a rift axis plays a more important role in driving magma laterally, rather than the topographic gradient along the ridge segment [e.g., *Rubin and Pollard*, 1987].

Recent studies of active arc volcanoes have improved our understanding of the way in which magma is moved laterally from central plumbing systems and its significance with respect to eruption mechanisms. Hachijojima volcano in the Izu-Bonin arc has two distinct lateral magma transport pathways, with dikes emanating from separate deeper and shallower crustal reservoirs. In contrast, Izu-Oshima volcano has only evidence for of lateral transport from a single magma chamber in the upper crust [*Ishizuka et al*., 2008, 2014]. Miyakejima erupted in 2000 and provided a spectacular example of lateral magma transport draining the magma reservoir, triggering caldera collapse, and generating violent explosive eruptions [*Geshi et al*., 2002].

These examples indicate that there are some key differences in the mode of lateral transport and in the composition of magmas involved. Investigating such magma movement is important not only to appreciate the processes occurring in the magmatic plumbing but also to understand the evolution of the volcanic edifice in relation to hazard mitigation. However, studying the physical and chemical properties of magma transport in active volcanic systems is difficult because most of the transported material resides at inaccessible crustal depths. Hence, this study set out to examine magma movement in a system where the transport pathways and the center of magmatic system are both exposed at the surface. Such a system is found as an extensive dike swarm extending from the central complex of the Isle of Mull in the North Atlantic Igneous Province, providing an opportunity to tie together the physical and chemical parameters of magma distribution.

In this study, we acquired physical parameters to examine the magma movement and flow regime within the Mull dike swarm using preferred crystal orientations and flow marks on dike surfaces. Chemical analysis of more than 200 dikes for high-precision radiogenic isotopes and whole rock chemistry enabled us to examine the compositional variation along and between the dikes at different distances from the Mull center. Based on these data, in combination with previously published analyses, the petrogenetic evolution and transport of dike magmas in the crust are explored.

2. Geological Background

2.1. Mull Central Complex

The Isle of Mull, off the west coast of Scotland, exposes a central volcanic complex that is part of the North Atlantic Igneous Province (Figure 1). Volcanism in this igneous province generated flood basalts initiated by decompression melting of the Icelandic mantle plume as it arrived at the base of the lithosphere at 61 Ma [e.g., *White*, 1988; *Saunders et al*., 1997; *Kent and Fitton*, 2000].

Crustal material through which the Mull central complex intruded has been constrained by surface exposure, xenolithic material, and geophysical data (summarized in *Thompson et al*. [1986]). The lower crust is consistent with granulite facies Archean Lewisian gneiss, while amphibolite facies Lewisian calc-alkaline

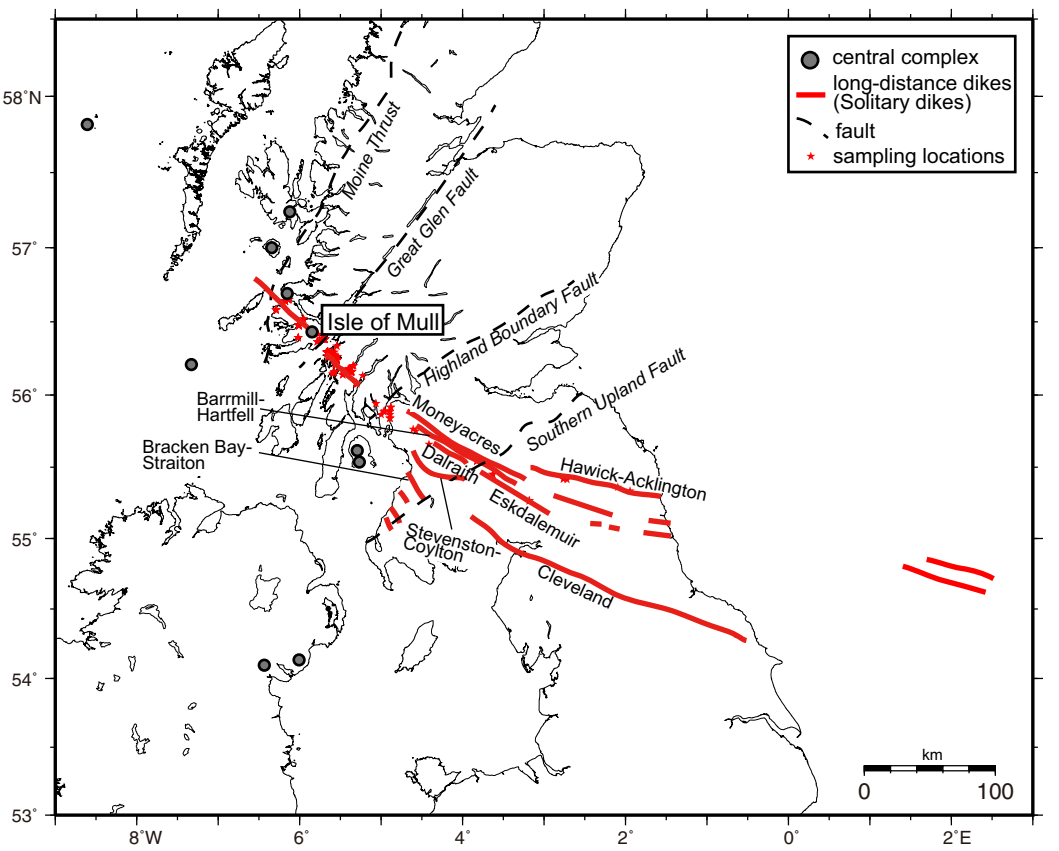

Figure 1. Locality map of dikes extending from Mull. Names and traces of dikes are after *MacDonald et al.* [2015].

orthogneisses may be a constituent of the middle crust. These are overthrust by upper crustal rocks comprising Proterozoic Moine metasedimentary rocks consisting of psammites and pelites, which are in turn overlain by a thin Mesozoic sedimentary rock sequence. The basement below Mull changes markedly across the Great Glen fault that cuts through southeasterly edge of Mull (Figure 3a). North of this fault is mainly composed of an Archean Lewisian gneiss and Moine schists, while south of this fault has Early Proterozoic basement and Dalradian metamorphosed sedimentary rocks [e.g., *Smith and Watson*, 1983] (Figures 3a and 3b).

The Mull central complex was first described in detail by *Bailey et al.* [1924], with more recent investigations detailing the igneous stratigraphy [*Kerr et al.*, 1999]. Volcanism has been divided into four stratigraphic stages (summarized in Figure 2), which from lower to upper levels are Mull Plateau Group (MPG) [*Morrison et al.*, 1980], Coire Gorm [*Kerr*, 1995], Central Mull Tholeiite (CMT) [*Kerr*, 1995], and Late Mull type [*Kerr et al.*, 1999]. MPG has been further subdivided into nine subtypes based on chemical characteristics, with the Staffa magma subtype being the oldest among MPG subtypes [*Kerr et al.*, 1999]. *Mussett* [1986] reported $^{40}Ar/^{39}Ar$ ages of 60 $\pm$ 0.5 Ma for MPG. Coire Gorm lavas overlie MPG, and uppermost MPG lavas are intercalated with the lowermost Coire Gorm flows [*Kerr et al.*, 1999]. These three stages of volcanism were followed by Late Mull type basalt activity. The majority of Mull volcanism took place between 61 and 59 Ma, and emplacement of some late-stage dikes continued until approximately 58 Ma [*Chambers and Pringle*, 2001].

Three overlapping igneous centers define the root of the volcanic system (Figure 3b). These are Glen More (Center 1), Beinn Chaisgidle (Center 2), and Loch Ba (Center 3), which represent a consecutive shift in the magmatic focus to the northwest with time [*Skelhorn et al.*, 1969; *Kerr et al.*, 1999]. Intrusions associated with these centers range from gabbro to granite, and each is accompanied by basic to acidic cone sheets (Figure 3b) [*Bailey et al.*, 1924; *Thomson*, 1986; *Kerr et al.*, 1999]. The CMT lava associated with Center 1 was dated to be 59.05 $\pm$ 0.27 Ma, and Loch Ba ring dike (Center 3) has an age of 58.48 $\pm$ 0.18 Ma [*Chambers and*

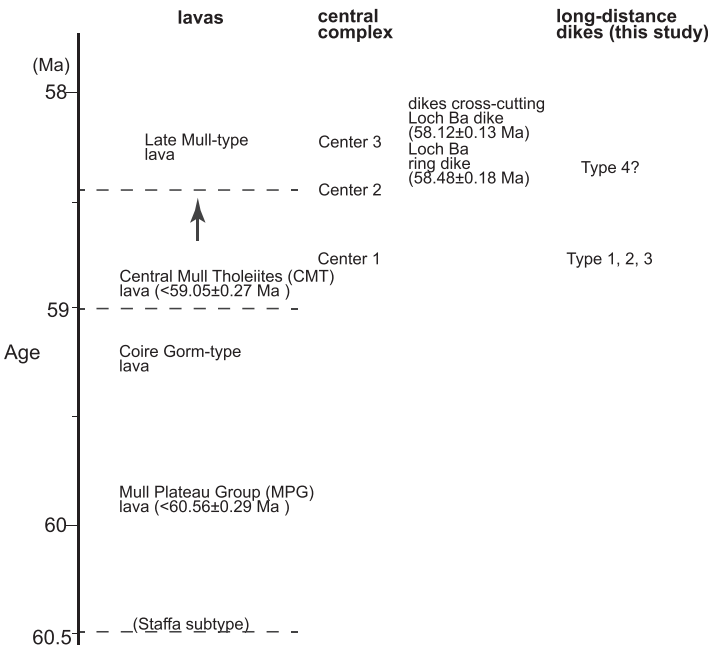

Figure 2. Summary of age relationships for the lava flows, central complexes, and dikes of Mull (modified after *Kerr et al*. [1999]).

Pringle, 2001] (Figure 2). These data clearly indicate that MPG including the oldest Staffa subtype predates activity of the central complex. *Kerr et al*. [1999] summarized that activities of Centers 1 and 2 overlap in age with CMT, and that the Late Mull type postdates Center 3 (Figure 2).

Geochemical characteristics of Mull basaltic magmas have changed through the evolution of the volcano. *Kerr et al*. [1999] highlighted variation in Sm/Yb, La/Nd, Ce/Y, and Ti/Zr ratios between the stages and suggested that the variation is caused by a change in the depth of partial melting with time, i.e., from deep melting at earliest MPG stage to shallower melting at Coire Gorm and CMT stages. This change in melting depth was explained by mechanisms such as a progressively thinning lithosphere [*Kerr*, 1994, 1995] and preferential extraction of melt from the top of a mantle column beneath lithosphere of a constant thickness [*Kerr et al*., 1999].

2.2. The Mull Dike Swarm

In the North Atlantic Igneous Province, the Mull and Skye central complexes fed extensive linear dike swarms [e.g., *Speight et al*., 1982, Figure 1]. Around Mull, the proximal dikes are dominated by planar sheets with diverse orientations and a mean of 140° [*Jolly and Sanderson*, 1995]. At greater distances, the number of dikes decreases and their thickness increases, while they retain strike directions between 130° and 150° [*Jolly and Sanderson*, 1995].

Holmes and Harwood [1929] recognized five definite lines and belts of tholeiitic dikes, including the Cleveland-Cockfield-Armathwaite dike in the north and Acklington dike in the south. *Tyrrell* [1917] and then *Holmes and Harwood* [1929] pointed out that the distribution and petrological affinities of these dikes indicated that they are an extension of the Mull swarm. *MacDonald et al*. [1988] reported that the Cleveland dike, one of the longest intrusions, appears to extend about 430 km from Mull to off the coast of northwest England and has chemical similarities to the tholeiitic rocks of Mull. On this basis, they concluded that the Cleveland dike is likely to have been fed by lateral migration of a Mull magma. *MacDonald et al*. [1988] also demonstrated that based on numerical modeling, lateral migration of magma at a relatively high speed (1–5 m/s) could emplace the Cleveland dike in 1–5 days with a small excess pressure in a relatively large magma chamber. Some of the longest dikes, such as Eskdalemuir, show a wide compositional range from tholeiitic basalt, through andesite, to rhyolite [*MacDonald et al*., 2009]. Since the rhyolite is of a similar composition to that associated with Mull Center 1, *MacDonald et al*. [2009] concluded that the felsic magma was also transported from Mull and mixed with tholeiitic basalt magma to produce the diverse compositional range, either at the exit from magma chamber or during lateral transport.

The timings of the Mull-derived dikes are relatively poorly constrained. *MacDonald et al*. [2010] suggested that the geochemistry of the dikes, such as the Cleveland dike, is similar to the MPG lavas with an age of 61–59 Ma. In contrast, *Kerr et al*. [1999] indicated that majority of the dike compositions belong to the CMT magma types, with minor amount of dikes having Coire Gorm-type compositions. There are also proximal basic dikes of Late Mull magma type crosscutting last major intrusives of Loch Ba [*Skelhorn et al*., 1969], whose age is estimated to be 58.12 ± 0.13 Ma by $^{40}Ar/^{39}Ar$ dating [*Chambers and Pringle*, 2001].

3. Sample Collection

Fieldwork was organized to examine the spatial variation of dike orientation and determine the direction of magma movement away from Mull. Samples of dikes at accessible distances were taken for elemental and isotopic analysis. Figure 3 shows the location of samples together with the major dikes on the simplified geological map of the southern Scotland and northern England. Dikes sampled in this study extend more than 270 km southeast from Mull (Cartington) and 30 km to the northwest. Physical data and samples were collected from 251 dikes as well as material from the host geological units which range from igneous rocks to sedimentary or metasedimentary rocks. Strike of the dikes is dominantly WNW-ESE to NNW-SSE, and their thickness ranges from 0.1 to 17 m.

Samples for geochemical analysis were obtained from most of the observed dikes and collected separately from the samples for intrusive direction analysis. Block samples were collected from the freshest part of the dikes. If suitable material for geochemical analysis could not be obtained by block sampling, core samples were recovered with an engine drill. Some locations where petrological variation was observed within single dike, block samples were collected from both margin and interior of the intrusion.

4. Analytical Methods

4.1. Determination of Magma Flow Direction

Some dikes exhibit preferred orientations via elongated vesicles and crystals. High cooling rates and high melt viscosities in the peripheral part of a dike favor the preservation of elongated vesicles, hence, the dike margins can be an indicator of the shearing direction during solidification [*Rust et al*., 2003]. Shear elongates vesicles along the deformation direction and forms an alignment of elongated vesicles subparallel to the flow band (Figure 4a). Shear also rotates elongated objects such as crystals and forms an oblique alignment. Therefore, the oblique alignment of crystals and vesicles relative to flow banding can indicate the direction of shear, which represents the movement of magma against the host rock [e.g., *Delaney and Pollard*, 1981; *Baer and Reches*, 1987; *Philpotts and Philpotts*, 2007]. Since the wall rock is fixed, shear deformation in the peripheral part of the dike indicates the flow direction of magma in the dike interior (Figures 4b and 4c).

We have only used the magmatic lineations observed in the outermost chilled margin of dikes for the analysis of intrusion direction, since they can record the magma movement against the host rock in the very early stages of dike intrusion. Magmatic lineations were recognized macroscopically in 24 dike outcrops at distances between 20 and 90 km from the Mull center (supporting information Table S1). The plunge and plunge direction of bubbles and crystals were measured by digital clinometer on the intrusion surface.

4.2. Whole Rock Chemistry

Two hundred twenty dike samples were analyzed for major and trace elements with selected samples also analyzed for Sr, Nd, and Pb isotope ratios. All the analytical work was conducted at the Geological Survey of Japan/AIST, and analytical data are listed in supporting information Table S2.

Normally, 50 g of rock chips were ultrasonically cleaned, and then pulverized using an agate mortar. Whole rock major elements were analyzed on glass beads, prepared by fusing 1:10 mixtures of 0.5 g subsamples and lithium tetraborate. The glass beads were analyzed using Panalytical Axios XRF spectrometers. External error and accuracy are generally $<$2%, but Na could have as much as $\sim$7% error depending on the surface condition of the glass beads. The data for each element agree with accepted values within these errors (supporting information Table S2).

The rare earth elements (REE), V, Cr, Ni, Rb, Sr, Y, Zr, Nb, Cs, Ba, Hf, Ta, Pb, Th, and U concentrations were analyzed by ICP-MS on a VG Platform instrument. About 100 mg of powder from each sample was dissolved in a HF-HNO_3 mixture (5:1) using screw-top Teflon beakers. After evaporation to dryness, the residues were redissolved with 2% HNO_3 prior to analysis. In and Re were used as internal standards, while JB2 with a similar level of dilution to the samples was used as an external standard during ICP-MS measurements. Instrument calibration was performed using five to six calibration solutions made from international rock standard materials (including BIR-1, BCR-1, AGV-1, JB1a, and BEN). Reproducibility is generally better than $\pm$4% (RSD) for the REE, and better than $\pm$6% (RSD) for other elements except those with very low concentration and Ni (see BHVO2 analysis in supporting information Table S2). Detection limits vary from element

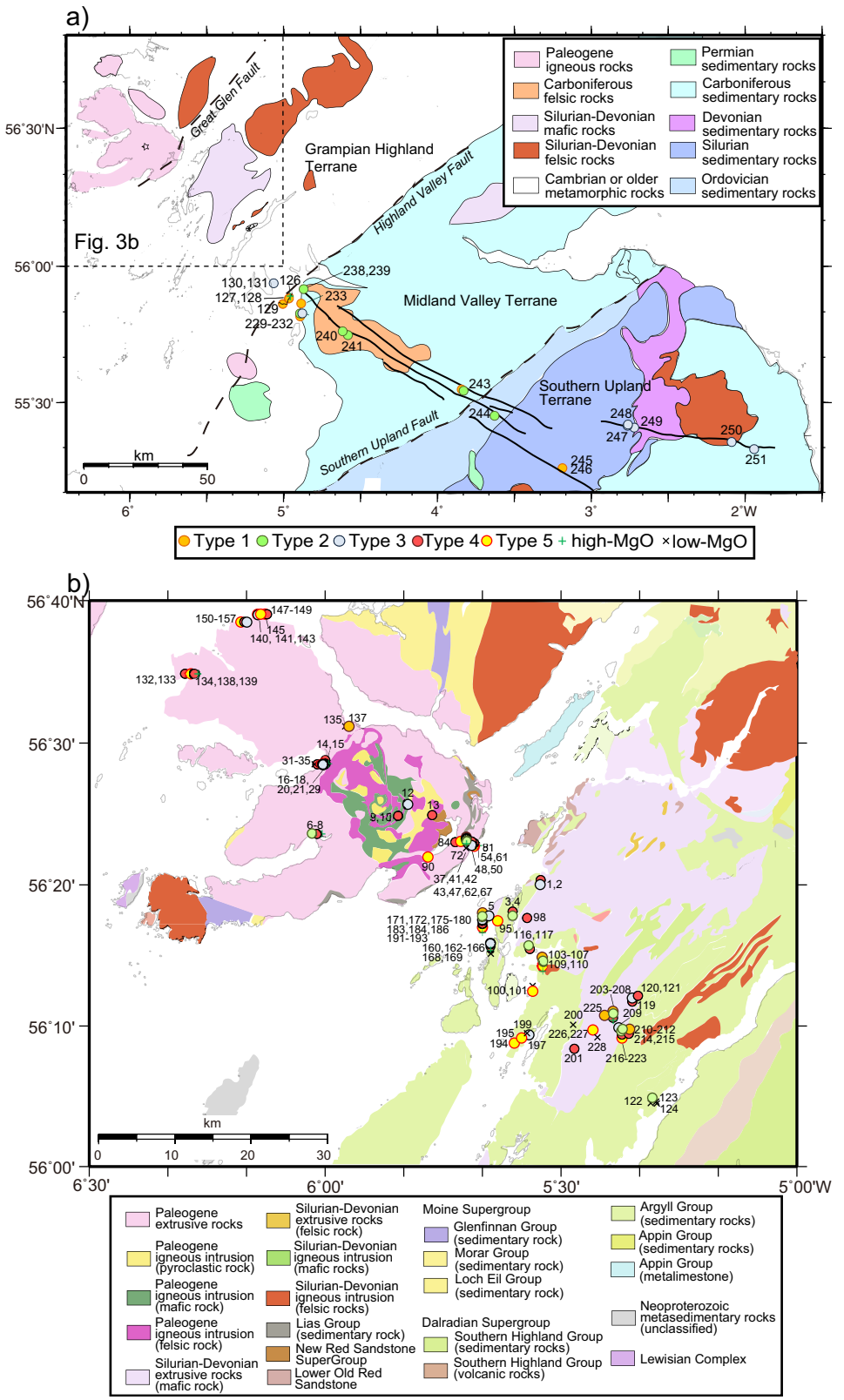

Figure 3. Sampling locations and numbers of dikes in this study. (a) Distal sampling locations from Mull with dike classification. (b) Sampling locations for relatively proximal sites imposed on a simplified geological map (from British Geological Survey).

.

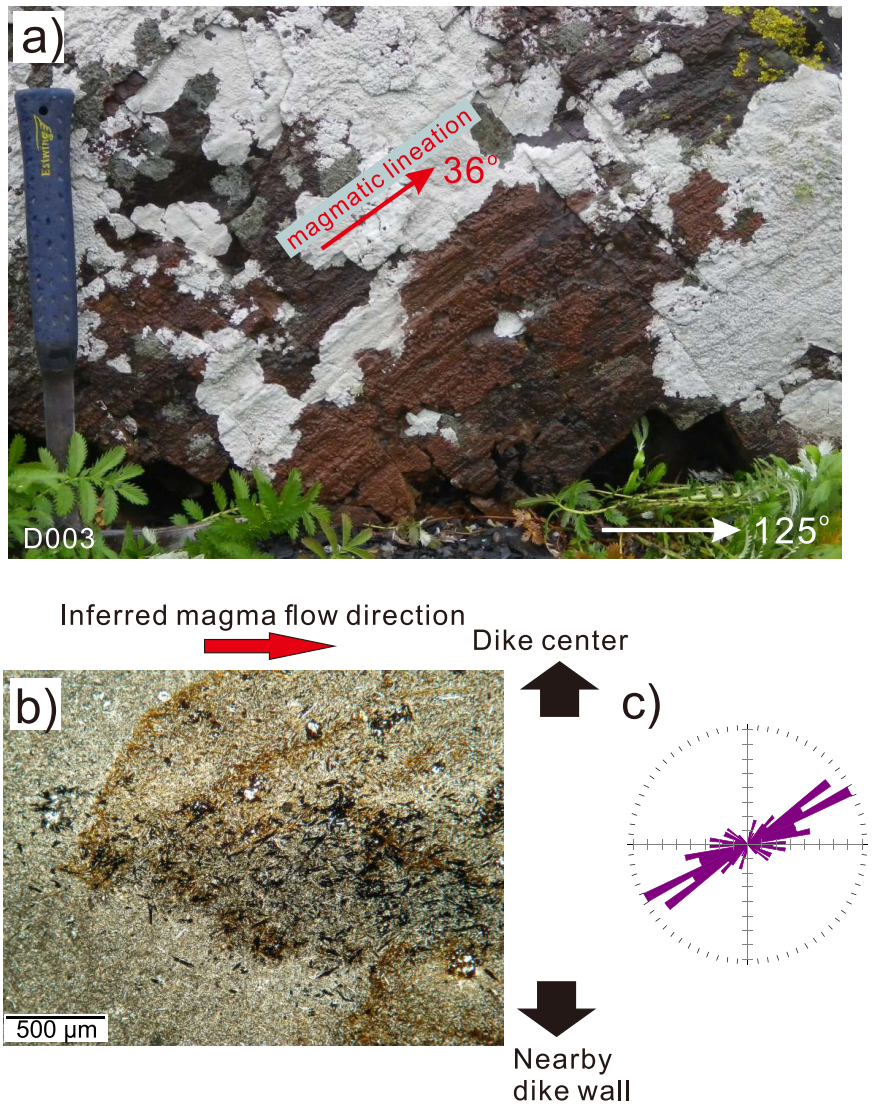

Figure 4. (a) An example of a magmatic lineation on the intrusion wall of dike D003, Seil Island, 22.6 km from the Mull center. The photograph shows the southern wall of dike D003, viewed from the outside. The orientation of the dike wall is 125° and vertical. (b) Photomicrograph taken parallel to the magmatic lineation and vertical to the dike wall. (c) Long axis orientation distribution of the opaque minerals in the photograph in Figure 4b.

to element, but for elements with low concentrations, such as REE and Ta, limits typically fall within a range from 0.2 to 2 pg g^{-1}.

4.3. Radiogenic Isotopic Composition

Isotopic compositions of Sr, Nd, and Pb were determined on 500 mg of hand-picked 0.5–1 mm rock chips. The chips were leached in 6 *M* HCl at 140°C for 30 min prior to dissolution in HF-HNO_3. Sr, Nd, and Pb isotope ratios were measured on a nine-collector VG Sector 54 mass spectrometer. Sr was isolated using Sr resin (Eichrom Industries, Illinois, USA). For Nd isotopic analysis, the REE were initially separated by cation exchange, before isolating Nd on Ln resin (Eichrom Industries, Illinois, USA) columns. Procedural Sr and Nd blanks were considered negligible relative to the amount of sample analyzed. Sr and Nd isotopic compositions were determined as the average of 150 ratios by measuring ion beam intensities in multidynamic collection mode. Isotope ratios were normalized to $^{86}Sr/^{88}Sr = 0.1194$ and $^{146}Nd/^{144}Nd = 0.7219$. Measured values for NBS SRM-987 and JNdi-1 [*Tanaka et al*., 2000] were $^{87}Sr/^{86}Sr = 0.710278 \pm 19$ (2 s.d., n =33) and

$^{143}Nd/^{144}Nd = 0.512104 \pm 10$ (2 s.d., n = 38) during the measurement period. All $^{87}Sr/^{86}Sr$ ratios were normalized to NBS SRM-987 $^{87}Sr/^{86}Sr = 0.710248$ [*Thirlwall*, 1991] as measured during the same analytical session.

Pb separation was achieved using AG1-X8 200-400 mesh anion exchange resin. Procedural Pb blanks were <30 pg and considered negligible relative to the amount of sample analyzed. Pb isotopic measurements were made in multidynamic collection mode using the double-spike technique (Southampton-Brest-Lead 207-204 spike SBL74) [*Ishizuka et al*., 2003; *Taylor et al*., 2015]. Natural (unspiked) measurements were made on 60–70% of collected Pb, giving ^{208}Pb beam intensities of 2.5–3 $\times 10^{-11}$A. Fractionation-corrected Pb isotopic compositions and internal errors were obtained by a closed-form linear double-spike deconvolution [*Johnson and Beard*, 1999]. The reproducibility of Pb isotopic measurement (external error: 2 s.d.) by double spike is <200 ppm for all $^{20x}Pb/^{204}Pb$ ratios. Measured values for NBS SRM-981 during the measurement period were $^{206}Pb/^{204}Pb = 16.9407 \pm 0.0039$, $^{207}Pb/^{204}Pb = 15.5010 \pm 0.0050$, and $^{208}Pb/^{204}Pb = 36.724 \pm 0.012$ (2 s.d., n = 21).

5. Results

5.1. Classification of Dikes

This study divides the dikes into seven groups (Types 1–5, low MgO, and high MgO), based on their geochemical characteristics (Table 1). It has been recognized that dikes extending from Mull have a diversity of Fe_2O_3/MgO at similar levels of MgO [*MacDonald et al*., 1988, 2010, 2014, 2015]. Such differences can be used to assess the relationship between each of the dike groups, as well as the potential comagmatic origins within and between the dikes, the Mull central complex and Mull lavas. This type of Fe-Mg distinction is shown in Figure 6a. Mull Plateau Group lavas (MPG) lie to the high-MgO end of a tholeiitic Fe-enrichment trend. Coire Gorm-type lavas extend to higher Fe_2O_3, while some of the CMT lavas show lower Fe_2O_3 than MPG at comparable MgO. The Fe-enrichment trend of MPG is continued to low MgO by Mull Center 3 [*Thomson*, 1986]. In contrast, Mull Center 1 forms an array with continuously declining Fe_2O_3 with less than 8% MgO: more akin to a calc-alkaline trend. Mull Center 2 is somewhat intermediate between Centers 1 and 3.

Overall, the range of MgO-Fe_2O_3 in the studied dikes roughly matches the diversity of compositions observed on Mull (Figure 6b). There are some differences, for example, the dikes do not extend to as high MgO (>10 wt %) as the MPG or have the most extreme Fe-enrichment observed in Center 3. Our new data include dikes with high Fe_2O_3 values relative to the published data (Figure 6b). This is because previously published dike data are mostly for long-distance dikes which show decreasing Fe_2O_3 with decreasing MgO, while our data include a number of proximal dikes which show first increasing, then decreasing Fe_2O_3 with decreasing MgO [*Dagley et al*., 2008; *MacDonald et al*., 1988, 2010, 2014, 2015].

At distances of >50 km from Mull, individual dikes can be traced across southern Scotland and northern England for >400 km [*Dagley et al*., 2008; *MacDonald et al*., 2010, 2015]. Figure 6c combines the data from this study with existing data for these distal individual dikes, which tend to fall naturally into three/four groupings [*MacDonald et al*., 1988, 2009, 2010, 2014; *Dagley et al*., 2008]. Each group represents a magma fractionation pathway or potentially a mixing trajectory between mafic and felsic magmas. Although these trajectories tend to focus toward an approximately similar low-MgO composition, they spread to a variety of Fe_2O_3 at their high-MgO end (Figure 6b). As such, it is possible to quantify the variation in the Fe_2O_3 by using the $Fe_{8.0}$ parameter, modified after *Klein and Langmuir* [1987]. Essentially this translates any

Table 1. Summary of Characteristics of Each Type of Dikes

	Type 1	Type 2	Type 3	Type 4	Type 5	High MgO	Low MgO
Number of dikes	20	29	36	38	27	19	14
MgO (wt %)[a]	2.5–7.5	2.5–7.5	2.5–7.5	2.5–7.5	2.5–7.5	>7.5	<2.5
SiO_2 (wt %)[a]	47.6–61.8	48.2–62.0	46.7–59.3	46.8–54.9	45.4–54.0	45.6–50.4	56.3–69.5
$Fe_{8.0}$	<12	12–13.4	13.4–16.1	<16.1	11.54–19.84	9.69–13.66	8.91–21.04
Th/Nb	>0.1	>0.1	>0.1	>0.1	<0.1	>0.1	>0.1
Distance from Mull (km)	12.7–275.1	9.7–273.5	3.6–399.3	3.4–155.1	8.9–44.1	9.2–90.2	9.2–53.5
Inclination of magma flow direction (°)	15	0–32	0–65	12–36	2–21		3–29

[a]Normalized value to total = 100%

composition along a magmatic trend of constant gradient to a fixed value of 8 wt % MgO. Figure 6c shows the division of the dike magmas into four types (Types 1–4 with increasing $Fe_{8.0}$), bounded by $Fe_{8.0}$ of 12%, 13.4%, and 16.1% (Figure 6c and Table 1). As the dike trajectories may represent mixing and because there is convergence at low MgO, the $Fe_{8.0}$ parameter is only meaningful for compositions between 2.5 and 7.5 wt % MgO. This range is represented by the shaded region in Figure 6c, and dike samples with MgO wt % higher than 7.5% are labeled as "high MgO" and those with lower than 2.5 wt % are labeled as "low MgO" (Figure 6b and Table 1). Type 1–4 dikes include previously reported long-distance dikes [*MacDonald et al*., 1988, 2009, 2010, 2014]. Type 1 dikes includes part of Eskdalemuir and Stevenston-Coylton dikes, Type 2 includes Moneyacres and Barrmill-Hartfell, Type 3 includes Cleveland, Dalraith, and Hawick-Acklington, and Type 4 includes Bracken Bay-Straiton (Figures 2 and 3).

Type 5 dikes have distinct geochemical characteristics relative to the other dikes. Their key distinguishing feature is that they have characteristically low Th/Nb regardless of MgO (ranging from ∼3 to 10 wt %; Figure 7) and are consequently defined by having Th/Nb less than 0.1 (Table 1).

There is some evidence that the distribution of dike types has some dependency on the distance from Mull, as shown in Figure 8. Type 5 dikes occur exclusively within 50 km from the Mull center, and "high-MgO" dikes only occur within 100 km. Type 4 dikes occur mostly within 50 km, although the Bracken Bay-Straiton dike [*MacDonald et al*., 2014] at 140–155 km from Mull is an exception. Types 1–3 occur along the entire length of the dike system.

Taking the dikes as a whole, many geochemical parameters, in particular the major elements, have a discernable systematic spatial variation (Figure 8). Distal dikes (>100 km) have a narrow range of compositions, while proximal dikes cover a much wider range. This change can be perceived as progressive with distance rather than being a step-function. For example, the SiO_2 content of dikes progressively narrows and converges on an andesitic composition with increasing distance from Mull, while basalt and rhyolite are restricted to proximal locations (Figure 8b). Distal dikes of each type have narrow major element compositional range, which is mainly due to the very tight compositional range of each long-distance dike (Figure 8a).

Trace element and isotopic compositions also show a systematic variation with distance (Figures 8d–8f). In the case of $^{206}Pb/^{204}Pb$, for example, Type 1–3 dikes show a wider range in the proximal area (∼17–19) but mostly converge to the limited range of 18.0–18.6 for the dikes further than 100 km from Mull (Figure 8e). Similar progressive changes are observed for Th/Nb and $^{143}Nd/^{144}Nd$ (Figures 8d and 8f). Th/Nb narrows its range to 0.4–0.8 at >100 km, and $^{143}Nd/^{144}Nd$ also narrows to 0.5118–0.5122 compared to the proximal dikes.

5.2. Magma Flow Direction Within Dikes

The plunge angles of magmatic lineations vary depending on the distance from Mull (Table 1 and supporting information Table S1). The dikes with distance shorter than 30 km show wide variation in angles spanning from 0° to 65°, while dikes further than 30 km from Mull show lower angles than the shorter ones, and smaller range from 0° to 32°, with 4° and 8° for dikes further than 50 km (Figure 5). Most of the dikes with high angles are Types 4 and 5, with a range between 12° and 65° for Type 4, and between 2° and 21° for Type 5 (Table 1). All the dikes with magmatic lineations suggest upward and outward flow of magma relative to the center of Mull.

5.3. Petrography

A summary of the petrographic features of the analyzed samples is listed in supporting information Table S3. Most proximal dikes (with a distance less than 30 km from Mull) examined are aphyric to sparsely phyric

.

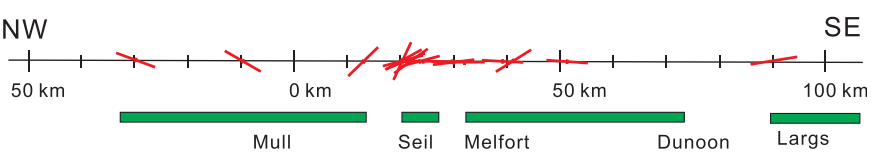

Figure 5. Magma flow direction within dikes recorded at distances relative to the Mull center: a location marked by the star on the map in Figure 3a.

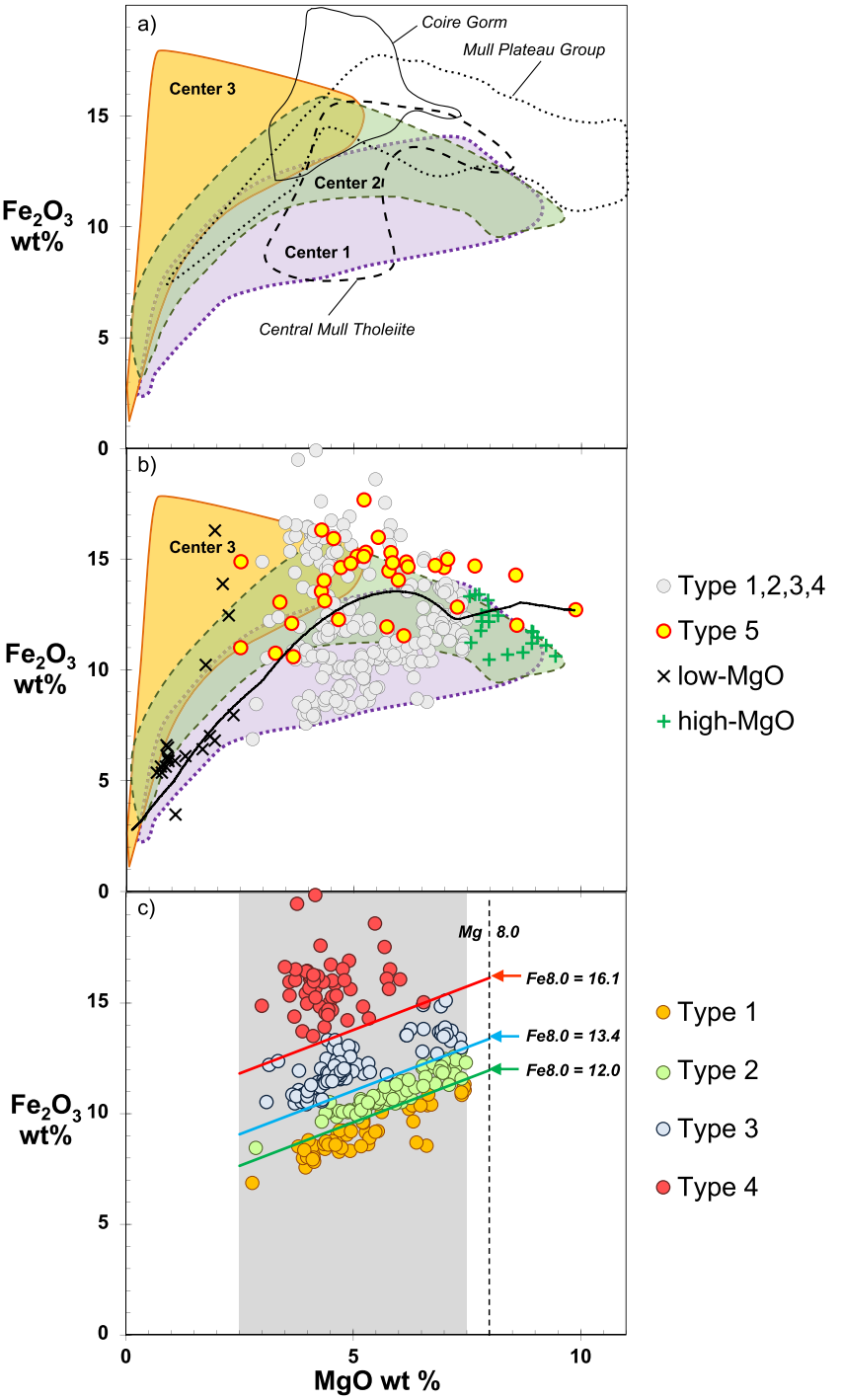

Figure 6. Classification of dikes based on MgO-Fe_2O_3 whole rock compositions. (a) Compositional ranges of Mull Plateau Group (MPG), Coire Gorm and Central Mull Tholeiite and Mull Centers 1–3 [*Kerr*, 1993; *Kerr et al.*, 1999], (b) highlights the dikes with low-MgO (<2.5 wt % MgO) and high-MgO (>7.5 wt % MgO) and Type 5 dikes (with Th/Nb < 0.1) relative to other Mull dikes. An example of fractionation path for a Type 5 dike (D156) is shown in black solid line. This is determined at 0.6 GPa and oxygen fugacity of 2 units above fayalite-magnetite-quartz buffer using (c) rhyolite-MELTS [*Gualda et al.*, 2012]. Subdivision of dikes with between 2.5 and 7.5 wt % MgO (gray shaded band) based on $Fe_{8.0}$: the Fe_2O_3 content recalculated back to MgO = 8 wt % following the procedure of *Klein and Langmuir* [1987]. Boundaries between Types 1–4 are shown in Figure 6c and are defined using a fractionation lines with slope = 0.786 as Type 1 = $Fe_{8.0}$ < 12.0, Type 2 = $Fe_{8.0}$ 12.0–13.4, Type 3 = $Fe_{8.0}$ 13.4–16.1, and Type 4 = $Fe_{8.0}$ > 16.1. Data include previously reported long-distance dikes [*MacDonald et al.*, 1988, 2009, 2010, 2014; *Dagley et al.*, 2008].

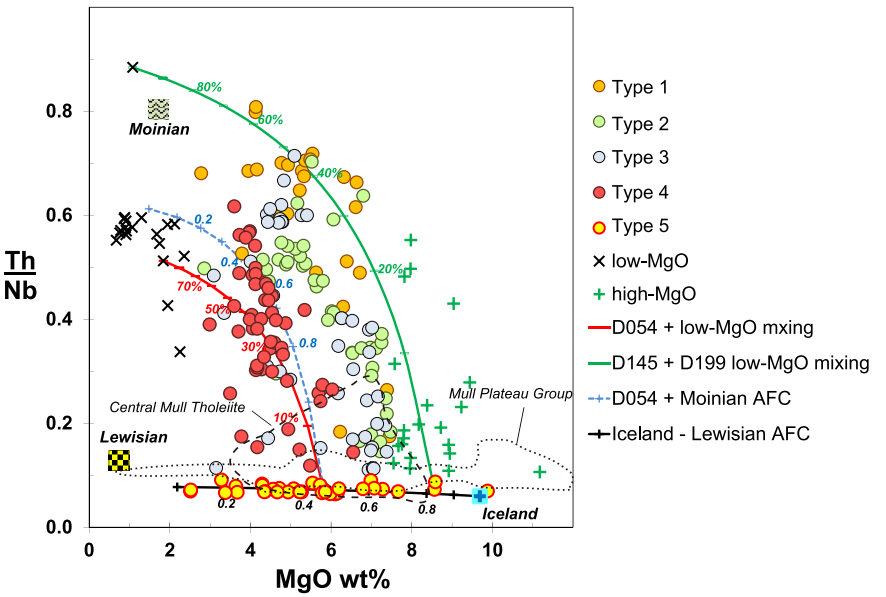

Figure 7. MgO-Th/Nb for Mull dikes divided according to Figure 6. Black line represents an assimilation-fractional crystallization (AFC) process [*DePaolo*, 1981] involving crystallization of a depleted Icelandic magma (Table 2) and the assimilation of a 20% melt of Lewisian granulite. The assimilation:crystallization ratio r = 0.1. Divisions along the line are (F), the fraction of melt remaining. Blue dashed line represents an example AFC trend involving the assimilation of a 10% melt of the average Moinian rock (Table 2) by a Type 5 magma (D054) with r = 0.2 at variable F. Crustal melting is calculated by modal melting using kd's from *Rollinson* [2012] and modal mineralogy for Lewisian granulite from *Rollinson* [2012] and for Moinian rocks from *Lambert* [1958]. Two example magma-mixing trends are shown. The green line represents mixing between Type 5 dike D145 and low-MgO dike D199; red line mixing between Type 5 dikes D054 and D199. Mixing increments are the % of low MgO added. Data for Central Mull Tholeiite (CMT) and Mull Plateau Group (MPG) are from *Kerr et al*. [1999].

basalt. Phenocrysts, where present, are dominantly plagioclase (2–5 mm, max 13 mm) accompanied by clinopyroxene (~2 mm) and olivine (~2 mm) in some cases. Dike D204 is picritic, having an exceptionally large amount of olivine phenocrysts (>15–20%). Some dikes are porphyritic (e.g., D164b, D178, D192, D199, D216a, D217, D219, D229, D230a, D230c, D233, and D242), mostly plagioclase phyric, but no particular petrological differences are noted with respect to distance from Mull.

Groundmass is dominantly composed of plagioclase, clinopyroxene, and opaque minerals, and olivine is also present in some basaltic dikes. Most of the Type 5 dikes contain olivine in their groundmass. Textures of these basalts vary between intersertal, variolitic, intergranular to ophitic/subophitic. Grain size varies from glassy, aphanitic to doleritic, and in some cases gabbroic in the central part of large dikes.

Most of the distal dikes are not basalt, but basaltic andesite to rhyolite. They are dominantly aphyric to sparsely plagioclase phyric, with intergranular/intersertal and occasionally ophitic/subophitic plagioclase and pyroxene. Grain size is commonly doleritic with minor amount of samples showing gabbroic or aphanitic texture.

Variable degrees of hydrothermal alteration are observed, mainly in proximal dikes. Patchy to pervasive chloritization is the most widely observed alteration of dikes on the Isle of Mull itself. Samples affected by significant hydrothermal alteration were excluded from further analyses.

5.4. Major and Trace Element Variations

Distinct trends are observed in the covariation of some elements. For example, the MgO versus SiO_2 plot (Figures 9a and 9b) has two trends: hyperbolic and straight. The straight trend, which shows relatively constant decrease in MgO with increasing SiO_2, is almost exclusively formed by distal, mostly Type 1–4 dikes. This straight trend overlaps with the compositions of Mull Center 1. A hyperbolic trend is most apparent in the MPG. Among the dikes, Type 5 shares its compositional range with MPG in having lower SiO_2 at a given MgO (Figure 9b). Overall, the combined trend of the MPG and Type 5 dikes is reproduced by a crystal fractionation path determined using rhyolite-MELTS [*Gualda et al*., 2012] using a relatively primitive Type 5 sample as the starting composition (black line in Figure 9b). Two distinct trends are also apparent on MgO

.

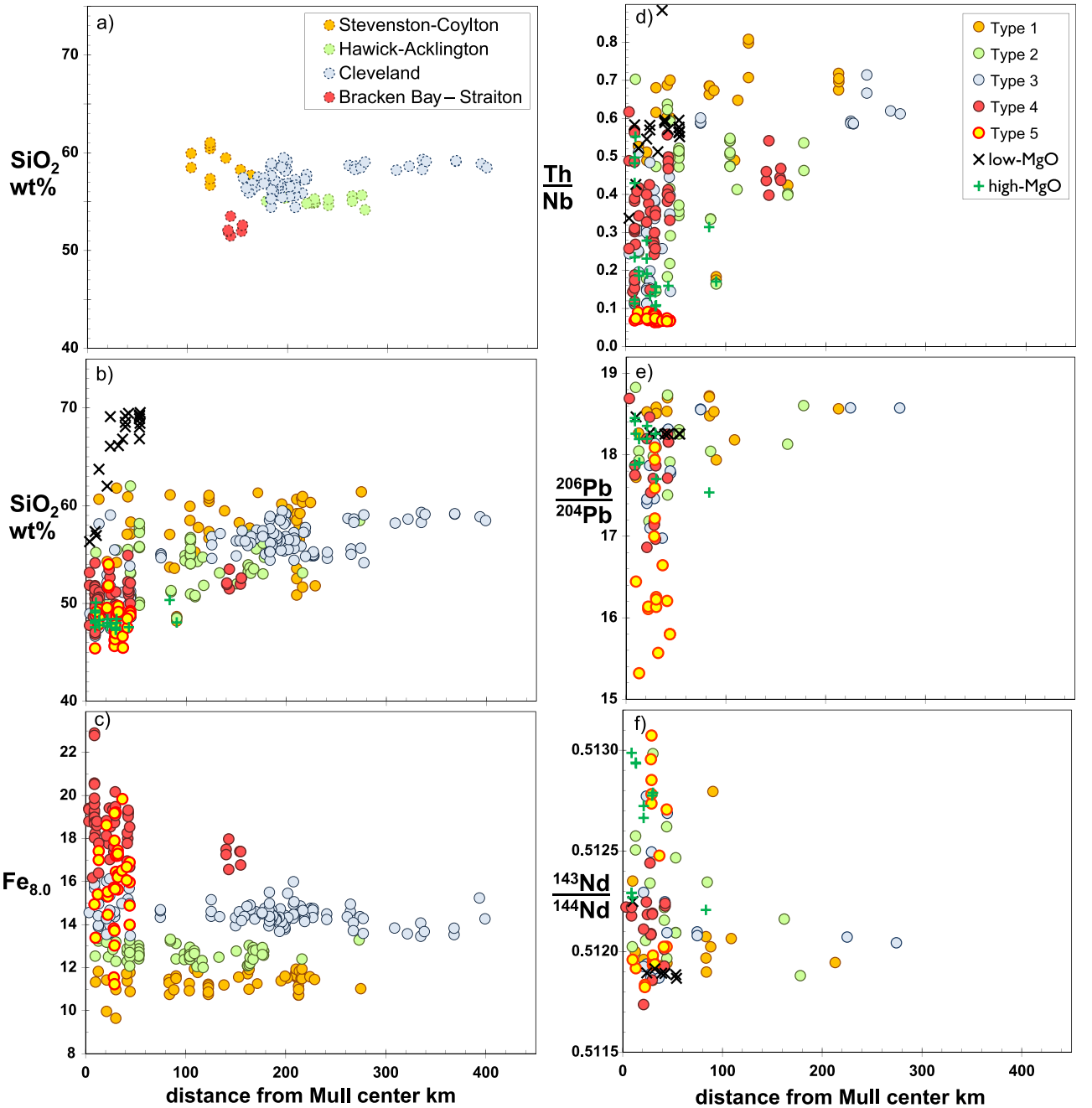

Figure 8. Compositional variation of dikes with distance from Mull. (a) SiO_2 for specific long-distance dikes—this study and data sources in Figure 6b. (b–f) Various parameters for all dikes divided according to Figure 6.

versus TiO_2 (Figure 9c). Types 1–3 form subhorizontal trends with constant TiO_2 and MgO ranging from 7.5% to 3.5%: again overlapping the field of Mull Center 1. Alternately, Type 5 dikes display a sharp increase in TiO_2 with increasing MgO, and reach a maximum at ~4% MgO (Figure 9c), with their compositional range comparable with the MPG. This Type 5 trend is again reproduced by the calculated fractionation path (Figure 9c).

Trace element ratio diagrams are also found to discriminate between the dike groupings (Figure 10). For example, on the Th/La-Nb/La plot (Figures 10b and 10c), Type 5 dikes show a tight positive correlation aligned between depleted Icelandic magma (high Nb/La with low Th/La: Table 2) and Lewisian granulitic crust (low Nb/La with very low Th/La: Table 2). Type 1–4 dikes form a fan-shaped array extending from a

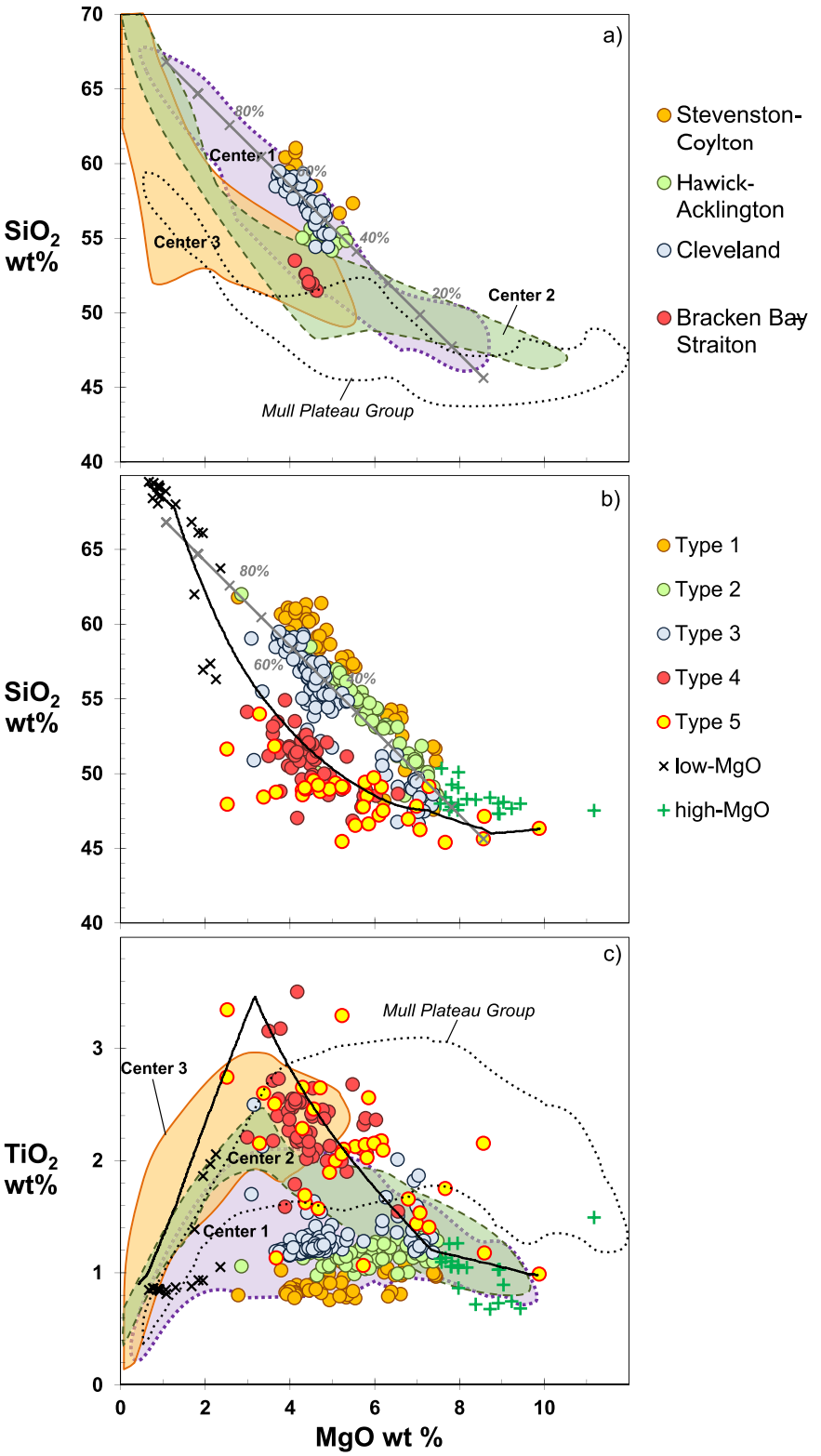

Figure 9. Major element variation of dikes: (a) MgO-SiO_2 for specific long-distance dykes—this study and data sources in Figure 6b, (b) MgO-SiO_2 for all dikes divided according to Figure 6, and (c) MgO-TiO_2. Black line in Figures 9b and 9c is a fractionation path for Type 5 dike (D156) using the same parameters as Figure 6b. The gray line with tick marks shows an example of magma mixing between a Type 5 dike D145 and a low-MgO magma; divisions in % of low MgO. Other data sources as for Figure 6.

.

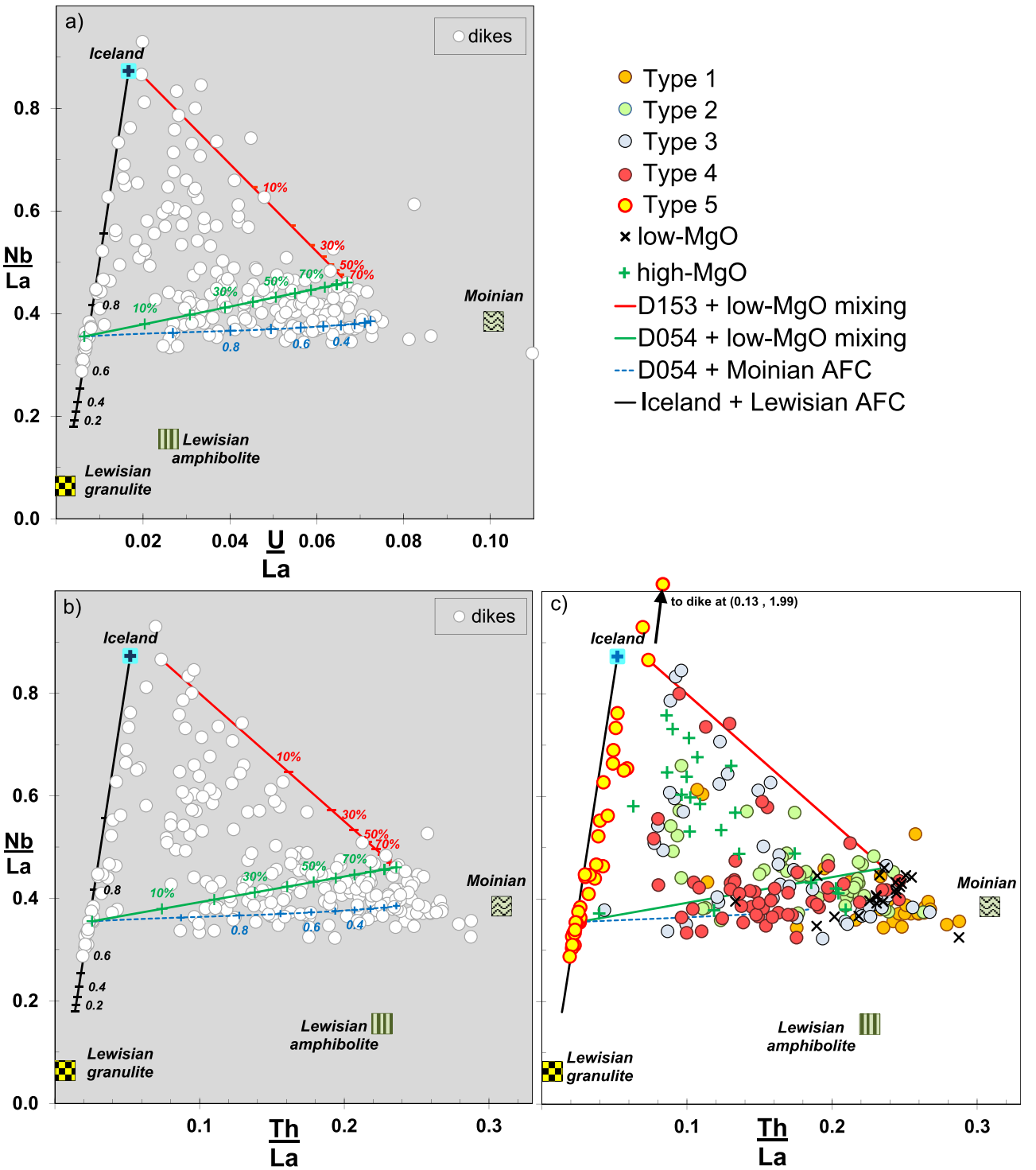

Figure 10. Trace element ratios for Mull dikes. (a) U/La-Nb/La and (b, c) Th/La-Nb/La. All AFC and mixing parameters shown here are calculated as for Figure 7.

similar range in Nb/La and converging toward an average Moinian rock composition at high Th/La. This trend is mirrored by an increasing Th/La from the high-MgO dikes to the low-MgO dikes. Type 1–4 dikes are distributed within a Icelandic magma-Lewisian granulite-Moinian rock triangle (Figures 10b and 10c), and this is also the case for U/La-Nb/La plot (Figure 10a).

Table 2. End-Member Components Used in Isotopic and Trace Element Modeling

	Depleted Icelandic Lava[a]	Lewisian Gneiss[b] (Granulite)	Lewisian Gneiss[c] (Amphibolite)	Moinian Rocks[d]
Major Elements (wt %)				
SiO_2	48.02	72.07	70.20	66.73
MgO	11.6	0.59	4.29	1.73
Trace Elements (ppm)				
Sr	46.0	515	475	261
Nb	0.53	2.64	3.9	16.6
La	0.54	41.6	24.8	44.9
Ce	1.6	95.9	44.6	83.1
Nd	1.9	36.9	17.7	36.9
Sm	0.88	6.51	2.70	7.21
Pb	0.073	6.93	11.2	25.7
Th	0.033	0.303	5.6	13.9
U	0.011	0.085	0.64	5.01
Isotope Ratios				
$^{87}Sr/^{86}Sr$	0.702888	0.71003	0.71168	0.72897
$^{143}Nd/^{144}Nd$	0.51315	0.51058	0.51077	0.51179
$^{206}Pb/^{204}Pb$	18.48	14.51	14.83	19.11
$^{207}Pb/^{204}Pb$	15.47	14.90	14.71	15.65
$^{208}Pb/^{204}Pb$	38.12	34.36	37.39	38.71

[a]Element abundance is from BIR-1 rock standard, except Pb concentration and isotope ratios which are from the equivalent depleted Iceland sample RP95C from *Gee et al*. [1998] and *Thirlwall et al*. [2004]. Th data for depleted Iceland assume Th/U of RP95C is equivalent to BIR-1 value of 3.556.

[b]Average granulite facies Lewisian gneiss were compiled from *Walsh et al*. [1979], *Whitehouse* [1990], *Whitehouse and Robertson* [1995], *Meyer et al*. [2009], and *Rollinson* [2012].

[c]Amphibolite facies Lewisian gneiss were compiled from *Walsh et al*. [1979], *Whitehouse* [1990], *Whitehouse and Robertson* [1995], *Meyer et al*. [2009], and *Rollinson* [2012].

[d]Average of Moine schist composition reported by *Pankhurst et al*. [1978], *Thompson et al*. [1986], and *Geldmacher et al*. [1998, 2002].

It has been reported that Lewisian gneisses of granulite facies and amphibolite facies have different geochemical characteristics [e.g., *Dickin*, 1981; *Thompson et al*., 1986]. Geochemical discrimination between the granulite and amphibolite facies of Lewisian gneiss can be achieved based on U/La, Th/La ratios and Pb isotopes (Figure 10 and supporting information Figure S1). It is noted that on the U/La-Nb/La plot (Figure 10a), contributions from either granulite facies or amphibolite facies Lewisian combined with Moinian rocks and depleted Icelandic magma cover most of the compositional range of the dikes. However, on the Th/La-Nb/La plot, dikes with lower Th/La clearly require a contribution from a component with low Th/La (∼0.08, Figure 10b): equivalent to Lewisian granulite. Pb isotopes also reflect the different U/Th systematics of the granulite and amphibolite facies. This is apparent in the $^{206}Pb/^{204}Pb$-$\Delta^{208}Pb/^{204}Pb$ (supporting information Figure S1) where all of the dikes form a tight array that is colinear with Moinian, depleted Iceland and Lewisian granulite. Typical Lewisian amphibolite has higher $\Delta^{208}Pb/^{204}Pb$, reflecting its long-term Th/U enrichment and does not correspond to any isotopic correlations observed within the dikes.

5.5. Elemental Variation With Radiogenic Isotopes

Taken as a whole, the dikes produce correlations between Sr-Nd isotopes and SiO_2 (Figure 11); $^{87}Sr/^{86}Sr$ produces a linear, positive trend with SiO_2 (Figure 11a), while $^{143}Nd/^{144}Nd$ decreases with increasing SiO_2 (Figure 11b). Isotope-trace element variations also display systematic differences in the dike compositions. On the $^{206}Pb/^{204}Pb$-Th/Nb plot (Figure 12a), Type 5 dikes form a trend with variable $^{206}Pb/^{204}Pb$ at a consistently low Th/Nb. This alignment lies along a line between depleted Icelandic magma and granulite facies Lewisian gneiss (Figure 12a and Table 2). Types 1–4, along with the high-MgO and low-MgO dikes, form a contrary array to Type 5 in displaying a marked increase in Th/Nb at a more consistent $^{206}Pb/^{204}Pb$: again focusing on the Moinian composition.

Type 5 dikes, apart from two anomalous samples, form a trend with decreasing Ce/Pb and decreasing $^{206}Pb/^{204}Pb$ extending from mantle/Iceland-like ratios (Ce/Pb ∼ 25, $^{206}Pb/^{204}Pb$ ∼ 18) toward Lewisian gneiss ($^{206}Pb/^{204}Pb = 14$, Ce/Pb ∼ 6). Notably, on this plot, Type 1–4 dikes clearly form a separate group with low Ce/Pb and higher $^{206}Pb/^{204}Pb$ and are effectively displaced toward the Moinian apex of the Icelandic-Lewisian-Moinian triangle.

On a Pb-Nd isotope plot (Figure 13a), Type 1–4 dikes extend from high $^{143}Nd/^{144}Nd$ with $^{206}Pb/^{204}Pb$ ∼ 18, to lower $^{143}Nd/^{144}Nd$ (∼ 0.5118) with $^{206}Pb/^{204}Pb$ of 17.0–19.0. As such, this range lies in a sector defined by depleted Icelandic magma, Moinian rocks, and Lewisian gneiss. Type 1 and 2 dikes generally lie to the high $^{206}Pb/^{204}Pb$ side of this triangle with ratios generally >18.0. Type 5 dikes have consistently lower $^{206}Pb/^{204}Pb$ than Icelandic magma and form an array extending from Icelandic magma composition toward the low $^{206}Pb/^{204}Pb$ and $^{143}Nd/^{144}Nd$ composition of Lewisian gneiss. Sr-Nd isotopes (Figure 13b) show that

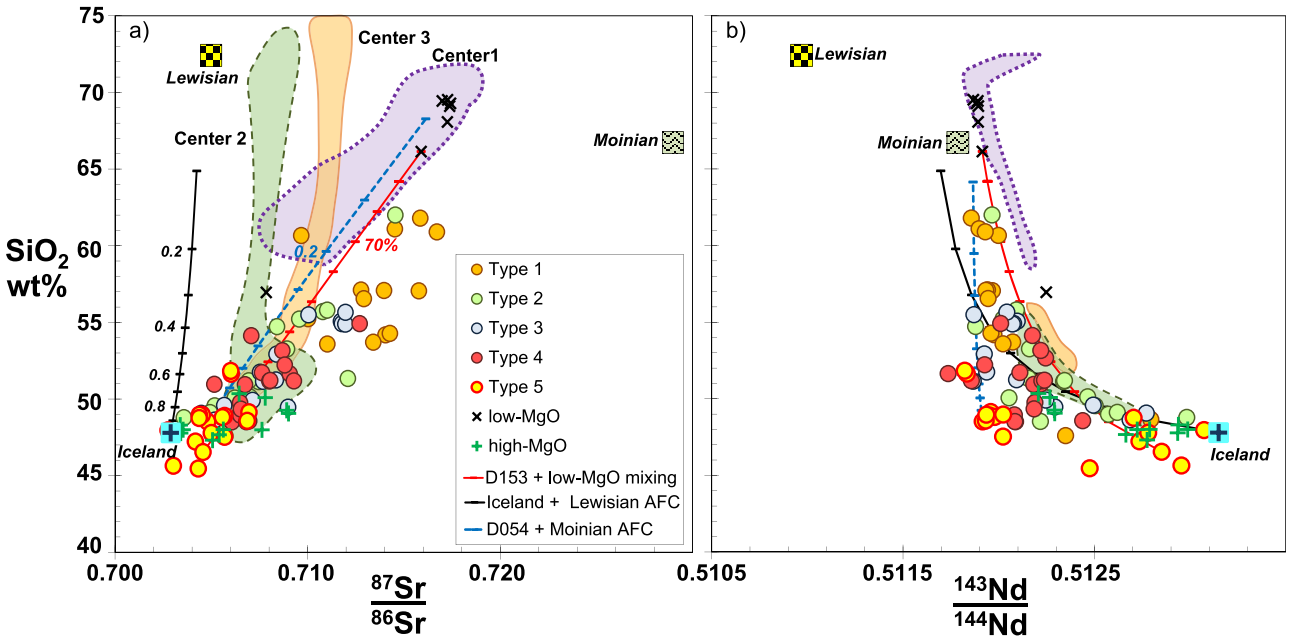

Figure 11. SiO_2 versus (a) $^{87}Sr/^{86}Sr$ and (b) $^{143}Nd/^{144}Nd$ for Mull dikes. Compositional fields are shown for Mull central complexes. Mixing and AFC trends calculated as for Figure 7.

Type 5 dikes have only a small increase in $^{87}Sr/^{86}Sr$ with decreasing $^{143}Nd/^{144}Nd$, while most of the Type 1–3 dikes show significant increases of $^{87}Sr/^{86}Sr$ with decreasing $^{143}Nd/^{144}Nd$.

6. Discussion

6.1. Lateral Magma Transport From Mull

To illustrate the direction and transport of magma within dikes extending from Mull, we have reconstructed the flow directions with distance from the volcanic center in Figure 5. Adjacent to the volcano, the dominant flow is near vertical or at a high angle to the surface both SE and NW of Mull, while beyond 30 km the flow direction is essentially horizontal. This evidence, combined with strike of dikes showing convergence toward Mull, leads us to conclude that the dikes southeast and northwest of Mull were fed by laterally transported magma. The near vertical transport of magma at distances of ~30 km does suggest that some of the dikes may either be sourced from a melt body outside the extent of the caldera system or were fed by lateral injection at depth, followed by vertical movement into a shallower fissure system (<10 km deep). Overall, the dikes are indicative of a magmatic origin beneath Mull central complex rather than being fed vertically from a series of magma chambers spread along the length of the dike system [*Speight et al*., 1982; *Dagley et al*., 2008]. The magma flow pattern from Mull is comparable to that reported from the Mackenzie dike swarm, where magma was injected vertically within 500 km of the central dike focus, then transported laterally for at least 2100 km [*Ernst and Baragar*, 1992].

6.2. Diking and the Evolution of the Mull Volcano

Evidence above indicates that the dike magmas originated beneath Mull, but our new geochemical data are able to shed some light on the different genetic pathways of the magmas and how they responded to residence in the crust.

MPG lavas, which form the main exposure of effusive volcanics, have a chemistry that reflects a contribution of Lewisian granulite to an asthenosphere-derived magma [e.g., *Morrison et al*., 1985; *Thompson et al*., 1982, 1986; *Kerr et al*., 1995, 1999]. In particular, this is reflected by the MPG array extending to low $^{206}Pb/^{204}Pb$ (around 15: Figures 12a and 12b) while retaining low mantle-like Th/Nb (around 0.05–0.1; Figure 12a). Following the MPG lavas, magmatic activity focused to the Mull central complex, which resulted in the Coire Gorm lavas, the CMT and the three effusive/plutonic volcanic centers. Sr and Nd isotopes of the Mull central

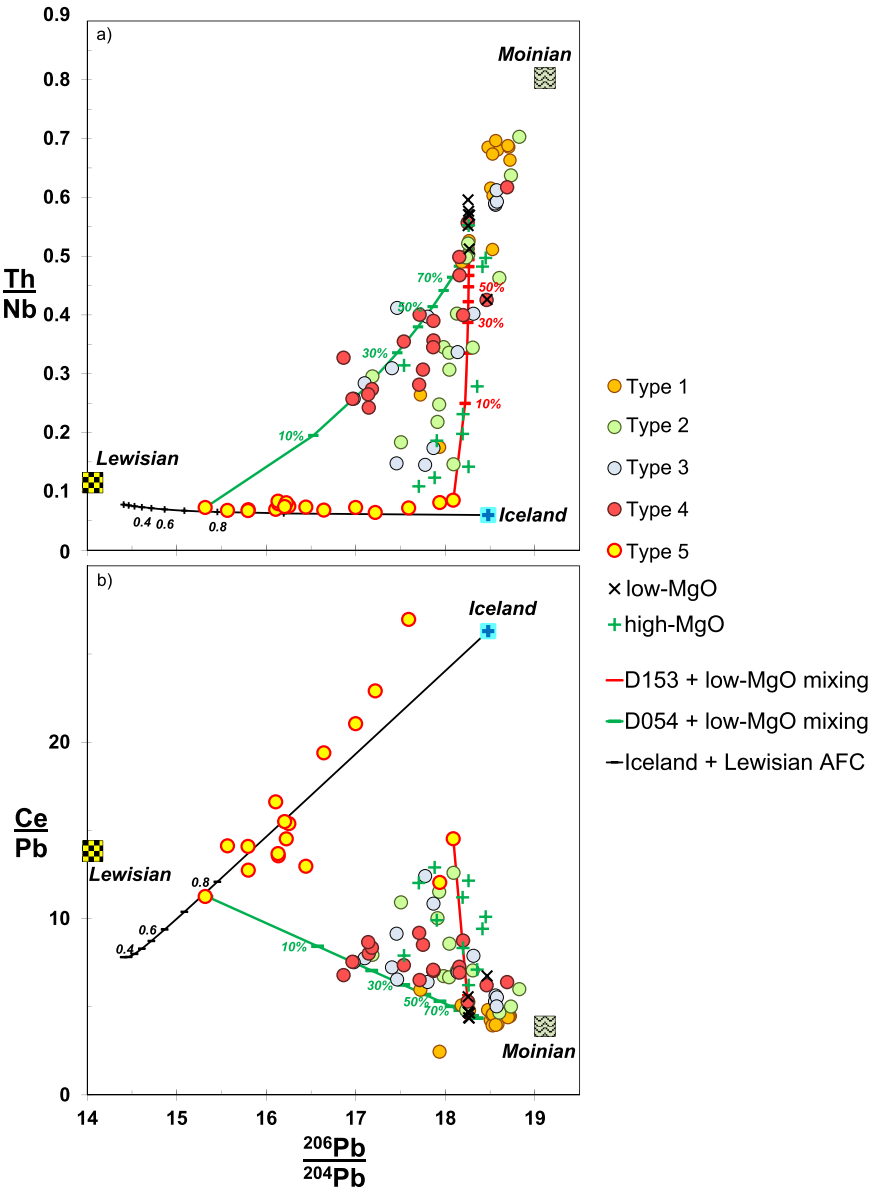

Figure 12. (a) $^{206}Pb/^{204}Pb$ versus Th/Nb and (b) $^{206}Pb/^{204}Pb$ versus Ce/Pb. Mixing and AFC trends calculated as for Figure 7.

complex form arrays which extend from asthenospheric mantle values toward very high $^{87}Sr/^{86}Sr$ (~0.718: Figure 11a) at moderate $^{143}Nd/^{144}Nd$ (0.5119: Figure 11b) [*Kerr et al.*, 1999]. These characteristics are compatible with the variable amount of assimilation of Moinian rocks (i.e., upper crust) which have significantly higher $^{87}Sr/^{86}Sr$ compared to Lewisian gneiss or asthenospheric mantle and lower $^{143}Nd/^{144}Nd$ than the mantle (Figures 11a and 11b). No Pb isotope data have yet been published for volcanics from the CMT lava, but our single data from a CMT lava indicate that $^{206}Pb/^{204}Pb$ remains high (~18.6: sample D090h01, supporting information Table S2) at a $^{143}Nd/^{144}Nd$ of 0.5126 (supporting information Table S2) which is compatible with a contribution from Moinian rocks.

Combining elemental and isotopic data allow us to evaluate the link between the dikes and events within the Mull volcano (Figure 1). Figures 6, 7, and 9−11 show the dikes separated into Types 1–5 and high/low MgO, as well as compared with the available Mull dataset. Type 5 dikes are seen to share the same low Th/Nb and equivalent variation in $^{206}Pb/^{204}Pb$ as the MPG lavas (Figure 12), whereas Types 1–4 seem to share

.

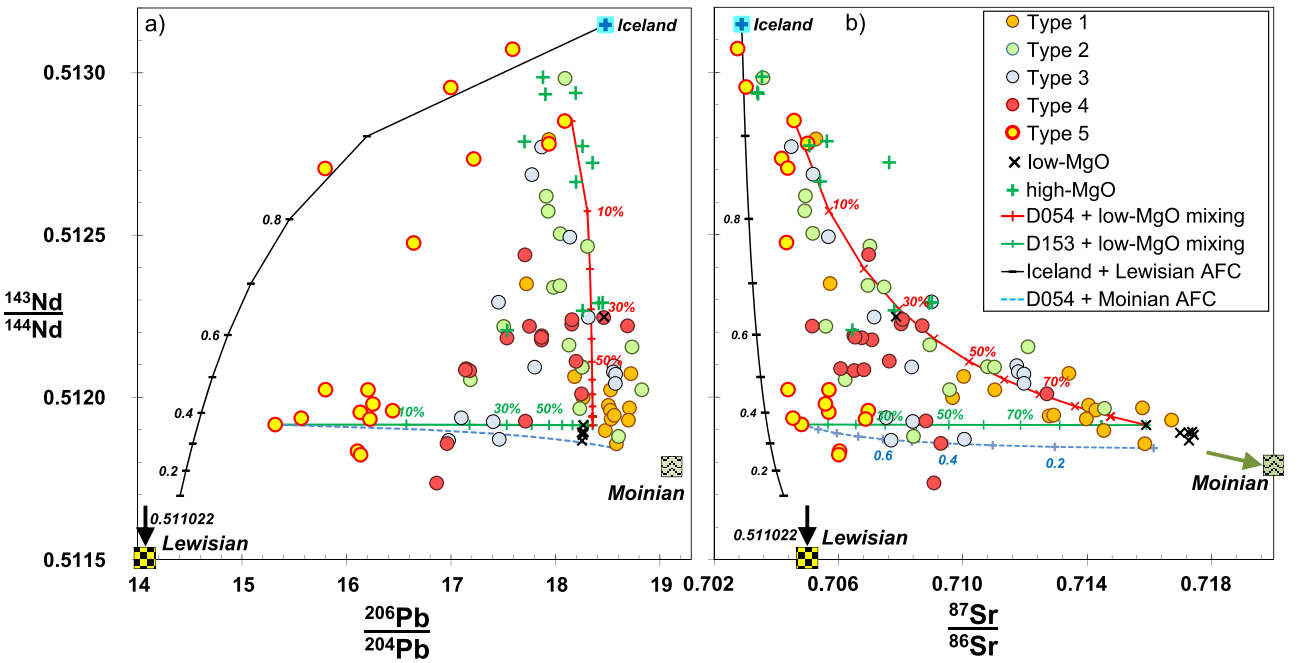

Figure 13. (a) $^{206}Pb/^{204}Pb$ versus $^{143}Nd/^{144}Nd$ and (b) $^{87}Sr/^{86}Sr$ versus $^{143}Nd/^{144}Nd$. Expected composition of upper crust (Moinian rocks) and lower crust (Lewisian granulite gneiss) are listed in Table 2. Mixing and AFC trends calculated as for Figure 7.

geochemical characteristics with the CMT (supporting information Table S2, not shown in the plots), indicative of contribution of Moinian rocks. Similar observations can be made in all of the trace element and isotope systematics for the dikes. These compositional differences indicate that the Type 5 and MPG magmas were the products of Lewisian contamination of a mantle-derived magma similar in composition to depleted Icelandic lavas. This contamination is best explained by up to 6–8% assimilation of a Lewisian granulite partial melt into the crystallizing magma: effectively an assimilation-fractional crystallization process (AFC) from a depleted Icelandic magma (Figures 7 and 10−13). The absolute amount of the crustal component depends on the fraction of crustal melting, crustal mineralogy, and the assimilant:crystallization ratio. As these are underconstrained in the Mull system there is some uncertainty in the amount of crust assimilated. These characteristics, shared with the majority of the MPG [e.g., *Kerr et al*., 1999], indicate that Type 5 magmas did not interact with upper crust after incorporation of lower crustal material. This lack of interaction indicates that Type 5 magmas bypassed any upper crustal reservoir, either on their way to a surface eruption or to produce a Type 5 dike (Figure 14).

In contrast, Types 1–4 as well as the Center 1 and CMT magmas appear to be contaminated by shallower Moinian rocks but still retain a legacy of Lewisian granulite addition (e.g., $^{206}Pb/^{204}Pb < 18$; Figure 12). To explain the composition of Type 1–4 dikes, we explore the interplay between AFC and magma-mixing processes. Type 1–4 dikes, especially distal ones, show good evidence for mixing between mafic and felsic magmas (Figures 6 and 9). Indeed, as the divisions between the Types 1–4 project back to progressively higher $Fe_{8.0}$ (Figure 6), the mafic magmas for each type effectively lie at successive points along a Type 5 or tholeiitic fractionation line. Magma mixing and AFC to produce the dike magma are further supported by relationship between MgO and Th/Nb (Figure 7). Type 4 dikes have lower MgO at a given Th/Nb than Types 1–3, yet cover an equivalent range of Th/Nb. They project back to the Type 5 array at MgO ∼ 6 wt %. Types 2 and 3 form a trend projecting back to MgO ∼ 7 wt %, while Type 1 and the high-MgO dikes project back to MgO ∼ 8 wt %. The red and green curves in Figure 7 provide examples of mixing between Type 5 magmas with different MgO and the low-MgO magma to illustrate that the Type 1–4 dikes can be generated by a variably fractionated Type 5 parent mixing with a low-MgO magma. It is also necessary to produce a significant volume of low-MgO magma to enable mixing to progress. Low-MgO dike compositions have Th/Nb

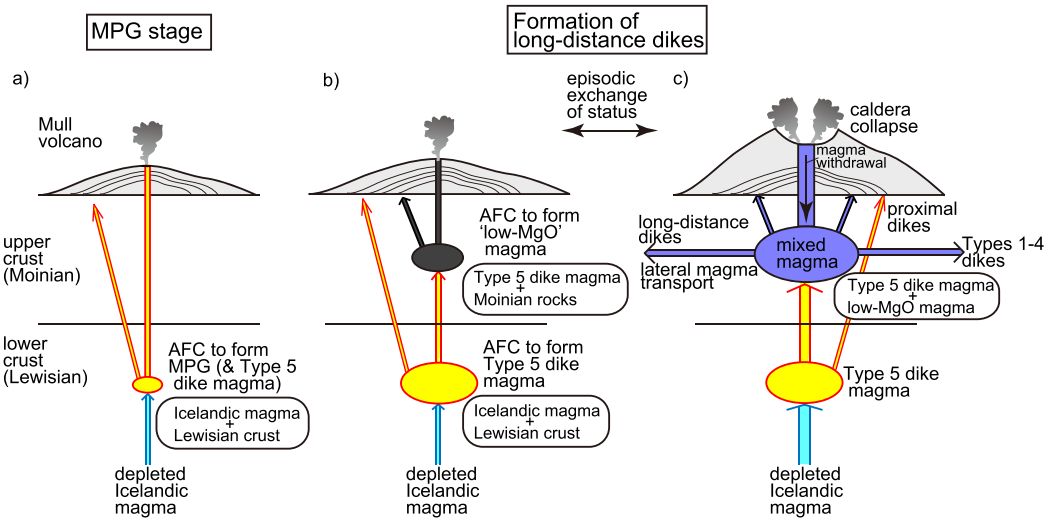

Figure 14. Schematic summary of Mull dike magma generation. (a) Magma plumbing during the Mull Plateau Group formation. The MPG magma supply from a mantle source similar to depleted Icelandic plume. Assimilation of Lewisian gneiss by AFC generates MPG and Type 5 magmas. Lack of a large magma reservoir may have allowed contaminated, but relatively unfractionated basaltic magma, to erupt. As envisaged by *Kerr et al*. [1999], Moinian contaminated magmatism was absent at this stage. Later magmatism envisaged for long-distance lateral magma transport and dike formation is shown in Figures 14b and 14c. (b) The formation of low-MgO magma in the upper crust. This magma was produced from a Type 5 or MPG parent that had already experienced assimilation of Lewisian in the lower crust and subsequently assimilated Moinian rocks during AFC in an upper crustal reservoir. Since Type 5 magmas tend to be more fractionated than MPG, they could have been stored in an enlarged lower crustal reservoir compared to earlier MPG magmas. (c) During long-distance diking events (Types 1–3), a large volume of Type 5 magma was transferred from the lower crust to the upper crustal reservoir. The result was a large volume (~80 km^3) of well-mixed Type 5 and low-MgO magmas in roughly equal proportions. This mixed magma eventually breached the reservoir wall and was transported laterally within upper crust. Evacuation of magma from the reservoir would cause withdrawal of magma from the main conduit and might have triggered caldera subsidence/collapse associated with Centers 1 and 2 in the Mull central complex. Type 5 dikes formed by intrusions directly from the lower crustal reservoir at a relatively high angle to the surface. These are likely to be lower-volume, proximal intrusions but potentially limited to outside the Mull magmatic center.

in the range 0.35–0.9 but are dominantly ~0.6. This is at the upper end of the range of Type 1–4 dikes and covers the average Moinian rock composition. Isotopically, the low-MgO magma requires the addition of the high $^{206}Pb/^{204}Pb$, $^{87}Sr/^{86}Sr$, and Th/Nb Moinian composition to the low $^{206}Pb/^{204}Pb$, $^{87}Sr/^{86}Sr$, and Th/Nb characteristics of Type 5. Hence, it is pertinent to consider an AFC process starting with a Type 5 magma which crystallizes and assimilates a partial melt of Moinian rocks (e.g., the blue dashed curves in Figures 7, 10, and 11).

If we adopt variably fractionated Type 5 magmas as the mafic end-members and mix with a low-MgO dike magma we can suitably generate Types 1–4. This is shown as the red and green mixing lines in Figures 7, 10, and 12. Some constraints on the amount of Type 5 magma and the low-MgO magmas are provided by the modeling shown in Figures 7 and 9−13, which indicate that the proportion of low-MgO magma is between 25 and 70%.

The temporal relationship between the dikes, Mull lavas, and the central complex is not clear. *MacDonald et al*. [2010] concluded that the dikes were related to the MPG event in the early development of the volcano (62–60 Ma). In contrast, *Kerr et al*. [1999] favored an origin coincident with the Mull central complex (59–57 Ma). Deductions about the temporal relationships between dikes and Mull volcanics are attempted here, however, there is scope to test these models by direct dating of the dikes. Similarity between their major element and isotopic compositions suggests that Type 1–3 dikes were contemporaneous with Center 1, while Type 4 dikes could be contemporaneous with Center 2 or 3 (Figures 1, 6, and 11). No igneous rocks with geochemical characteristics similar to the MPG have been reported at Center 1 or CMT stage, and the activities of Center 1 and CMT are stratigraphically positioned after the MPG [*Kerr et al*., 1999] (Figure 1). This implies that the difference between the MPG and Type 1–4 dikes was caused by a temporal shift in the composition of Mull and that all distal dikes formed after the MPG. Type 5 dikes share geochemical characteristics with the MPG in terms of the contribution of Lewisian gneiss (Figures 7 and 10−13). However, Type

5 dikes are slightly distinct from MPG because they have generally experienced greater amounts of fractional crystallization (Figures 6, 7, and 9). This implies that the Type 5 dike magmas either resided for longer in the lower crust or were part of a more extensive lower crustal reservoir compared to the MPG. An inference from the geochemical modeling shown in Figures 7 and 10−13 is that Type 5 magmas developed in the lower crust, rising episodically to feed an upper crustal reservoir. At this level, the magma could evolve further by AFC to produce low-MgO magmas or mix with preexisting upper crustal melts to produce Type 1–4 dikes. Accordingly, this equates to dike Types 1–5 all existing in the same magmatic stage, but with Type 5 dike magmas not erupting at the surface, or the surface record subsequently being lost. Type 5 contamination characteristics match the Lewisian lower crust and not the Moinian upper crust. Hence, it is possible that these Type 5 magmas either fed directly upward to be intercepted by, and mix with, the shallower magma reservoir, or laterally bypassed the upper reservoir to generate Type 5 dikes.

Constraints on the depth of magma storage can be gained from the location of the Moine-Lewisian interface. This boundary is a thrust dipping at ∼15° SE and breaks surface ∼30 km NW of Mull [*Magee*, 2011] and projects to a depth of ∼8 km beneath the volcanic center. It should be noted that since this estimate assumes that the dip of the thrust is constant, which may not be the case for a thrust of this scale, there is a large uncertainty in this depth. Contamination of magma with Lewisian gneiss indicates a residence in the crust at depths >8 km, while contamination of Moinian rocks involves interaction at <8 km. Consequently, if magmas have a Moinian rock signature then they must have had a final residence depth <8 km, or at least mixed with magmas at this depth prior to eruption or intrusion.

6.3. Magma Volumes of the Mull Dikes

Type 5 dikes are always basaltic, which potentially means that magma residence time in the crust was short, but sufficient to assimilate 4–7% Lewisian crust (Figures 7 and 10−13). As the maximum length of Type 5 intrusions is ∼50 km (with an average of 30 km), and with an average thickness around 2.6 m, the volume of magma involved would be 0.8–1.3 km^3 (assuming an average dike height of 10 km). Type 4 dikes are restricted to around 150 km long, representing volumes of up to 3.4 km^3. Type 1–3 dikes have the greatest volumes, extending 400–500 km with volumes 30–80 km^3, which is similar to the estimate for the Cleveland dike (Type 2) by *MacDonald et al*. [1988]. An observation from the relationship between SiO_2 and distance (Figure 8a) is that andesitic magma, rather than basaltic or rhyolitic, formed the longest and largest volume Type 1–3 dikes, and was perhaps the only magma available in suitable quantities to supply large-scale propagation events. *MacDonald et al*. [2010] proposed that the andesitic magma was a mixture between mafic and felsic components, either prior to or during dike intrusion. This is entirely reasonable and the evidence in this study indicates that they initiated as Type 5 basalts in the Lewisian lower crust followed by a mixing with an approximately equivalent volume of felsic magma in a shallower upper crustal reservoir (Figure 14). Combining the products of the lower and upper crustal reservoirs would generate the appropriate composition and volume required for the longest dikes.

Clearly the evacuation of large volumes of magma from a subvolcanic reservoir would have had ramifications for the Mull volcano. Evidence from Miyakejima volcano [*Geshi et al*., 2002] illustrates the explosivity caused by lateral transport of ∼1–2 km^3 of magma, hence, the withdrawal of 50–100 km^3 from a volcanic center is likely to produce significant caldera collapse and generate pyroclastic volcanism (Figure 14). There is evidence for multiple explosive events within the Mull central complex, such as the explosion breccias within Centers 1 and 2, which are associated with vent or caldera development [*Kerr et al*., 1999; *Emeleus and Bell*, 2005]. As discussed in the previous section, the large-volume Type 1–3 dikes are geochemically similar to Center 1 or 2 magmas and hence may have been coeval.

6.4. Crustal Contamination During Magma Transport

As dike magmas clearly experienced upper crustal assimilation, a question is whether this assimilation took place beneath the Mull volcano or during long-distance lateral transport? Among each type of dike, especially specific long-distance dikes (Figures 8 and 9), there seems to be little geochemical variation with distance from Mull indicative of a progressive assimilation of the host rock (Figure 8). For example, Type 1 and 2 dikes show similar and significant contribution of Moinian rocks regardless of the distance from Mull (Th/Nb in Figure 8d). This is despite the fact that the dikes in this study intrude many different geologic units and a great diversity of rock types in their transit across southern Scotland and northern England

[*MacDonald et al*., 1988]. This observation is in accord with the assimilation of both lower and upper crustal material beneath the Mull igneous center rather than during lateral magma movement.

Lack of interaction between host rocks and magma could be one of the factors that allowed magma to be transported great distances without freezing. Mull dikes may have propagated with similarly rapid magma movement to that observed in some recent diking events. For example, magma moving 30 km in 6 days away from Miyakejima prior to the July/August 2000 eruption, and ~30 km in about 4 days prior to the caldera collapse at Bárdarbunga volcano in 2014 [e.g., *Yamaoka et al*., 2005; *Gudmundsson et al*., 2016].

7. Conclusions

Magmatic lineations within dikes demonstrate that the direction of magma flow gradually changed from near vertical to horizontal within 30 km of the Mull central complex and provides firm evidence for lateral magma transport.

Geochemical correlations between the extensive Mull dike swarm and Mull volcanism indicate that long-distance magma transport initiated after the formation of the voluminous Mull Plateau Group lavas is likely to have been contemporaneous with the development of the Mull central complex. Short-distance dikes with low Th/Nb (Type 5) reflect contamination of a primary depleted Icelandic composition magma with Lewisian granulite in the lower crust and involve relatively low volumes of magma (<1 km^3). Type 5 magmas progressively fed into an upper crustal reservoir, where they crystallized and assimilated Moinian host rocks. The resultant low-MgO felsic magma was then combined in variable proportions with incoming volumes of Type 5 magma from the lower crust to produce the majority of the distal dikes. The longest dikes represent the episodic combination of a roughly equal proportion of basaltic Type 5 magma from the lower crust mixing with the felsic contents of the upper crustal reservoir. The resultant andesitic magma was of sufficient volume (between 30 and 80 km^3) to supply dikes of ~500 km length. These high volume magma evacuations from beneath the Mull volcano are likely to be responsible for the formation of calderas developed in the stages of Centers 1 and 2 [*Kerr et al*., 1999].

During the magma transport within crust, both crystallization and assimilation of the various country rocks appear to be minimal, with all crustal contamination taking place beneath the Mull volcano. This lack of interaction with the host rocks may have allowed magma to move long distances without freezing.

Acknowledgments
We thank K. Yamanobe for assistance with the ICP-MS measurements. This work was supported by JSPS bilateral grant (Japan-UK) and the Grant-in-Aid (B) (16740299) for O.I. The authors acknowledge the constructive reviews by T. Rooney, C. Magee, and A. Kerr and helpful editorial comments by J. Blichert-Toft which have greatly improved an earlier version of the manuscript. The data used are listed in the references and tables in main text and supporting information.

References

Aloisi, M., A. Bonaccorso, and S. Gambino (2006), Imaging composite dike propagation (Etna, 2002 case), *J. Geophys. Res.*, *111*, B06404, doi: 10.1029/2005JB003908.
Baer, G., and Z. Reches (1987), Flow patterns of magma in dikes, Makhtesh Ramon, Israel, *Geology*, *15*, 569–572.
Bailey, E. B., C. T. Clough, W. B. Wright, J. E. Richey, and G. V. Wilson (1924), Tertiary and post-Tertiary geology of Mull, Loch Aline and Oban, in *Memoir of the Geological Survey of Great Britain*, HMSO, Edinburgh.
Björnsson, A. (1985), Dynamics of crustal rifting in NE Iceland, *J. Geophys. Res.*, *90*, 10,151–10,162.
Chambers, L. M., and M. S. Pringle (2001), Age and duration of activity at the Isle of Mull Tertiary igneous centre, Scotland, and confirmation of the existence of subchrons during Anomaly 26r, *Earth Planet. Sci. Lett.*, *193*, 333–345.
Dagley, P., R. R. Skelhorn, A. E. Mussett, S. James, and J. N. Walsh (2008), The Cleveland dyke in southern Scotland, *Scott. J. Geol.*, *44*, 123–138, doi:10.1144/sjg44020123.
Delaney, P. T., and D. D. Pollard (1981), Deformation of host rock and flow of magma during growth of minette dikes and breccia-bearing intrusions near Ship Rock, New Mexico, *U.S. Geol. Surv. Prof. Pap.*, *1202*, 61 pp.
DePaolo, D. J. (1981), Trace element and isotopic effects of combined wallrock assimilation and fractional crystallization, *Earth Planet. Sci. Lett.*, *53*, 189–202.
Dickin, A. P. (1981), Isotope geochemistry of Tertiary igneous rocks from the Isle of Skye, NW Scotland, *J. Petrol.*, *22*, 155–189.
Dziak, R. P., C. G. Fox, and A. E. Schreiner (1995), The June-July 1993 seismo-acoustic event at CoAxial segment, Juan de Fuca Ridge: Evidence for a lateral dike injection, *Geophys. Res. Lett.*, *22*, 135–138.
Ebinger, C. J., and M. Casey (2001), Continental breakup in magmatic provinces: An Ethiopian example, *Geology*, *29*, 527–530.
Einarsson, P., and B. Brandsdottir (1980), Seismological evidence for lateral magma intrusion during the July 1978 deflation of the Krafla volcano in NE-Iceland, *J. Geophys.*, *47*, 60–65.
Emeleus, C. H., and B. R. Bell (2005), *British Regional Geology: The Palaeogene Volcanic Districts of Scotland*, 4th ed., Br. Geol. Surv., Keyworth, Nottingham, U. K.
Ernst, R. E., and W. R. A. Baragar (1992), Evidence from magnetic fabric for the flow pattern of magma in the MacKenzie giant radiating dyke swarm, *Nature*, *356*, 511–513.
Ernst, R. E., and K. L. Buchan (1997), Giant radiating dyke swarms: Their use in identifying Pre-Mesozoic large igneous provinces and mantle plumes, in *Large Igneous Provinces: Continental, Oceanic and Planetary Flood Volcanism*, edited by J. J. Mahoney and M. F. Coffin, pp. 297–334, AGU, Washington, D. C.

Gee, M. A. M., M. F. Thirlwall, R. N. Taylor, D. Lowry, and B. J. Murton (1998), Crustal processes: Major controls on Reykjanes Peninsula Lava Chemistry, SW Iceland, *J. Petrol.*, *39*, 819–839.
Geldmacher, J., K. M. Haase, C. W. Devey, and C. D. Garbe-Schönberg (1998), The petrogenesis of tertiary cone-sheets in Ardnamurchan, NW Scotland: Petrological and geochemical constraints on crustal contamination and partial melting, *Contrib. Mineral. Petrol.*, *131*, 196–209.
Geldmacher, J., V. R. Troll, C. H. Emeleus, and C. H. Donaldson (2002), Pb-isotope evidence for contrasting crustal contamination of primitive to evolved magmas from Ardnamurchan and Rum: Implications for the structure of the underlying crust, *Scott. J. Geol.*, *38*, 55–61.
Geshi, N., T. Shimano, T. Chiba, and S. Nakada (2002), Caldera collapse during the 2000 eruption of Miyakejima Volcano, Japan, *Bull. Volcanol.*, *64*, 55–68.
González, P. J., S. V. Samsonov, S. Pepe, K. F. Tiampo, P. Tizzani, F. Casu, J. Fernández, A. G. Camacho, and E. Sansosti (2013), Magma storage and migration associated with the 2011–2012 El Hierro eruption: Implications for crustal magmatic systems at oceanic island volcanoes, *J. Geophys. Res. Solid Earth*, *118*, 4361–4377, doi:10.1002/jgrb.50289.
Grandin, R., E. Jacques, A. Nercessian, A. Ayele, C. Doubre, A. Socquet, D. Keir, M. Kassim, A. Lemarchand, and G. C. P. King (2011), Seismicity during lateral dike propagation: Insights from new data in the recent Manda Hararo–Dabbahu rifting episode (Afar, Ethiopia), *Geochem. Geophys. Geosyst.*, *12*, Q04B08, doi:10.1029/2010GC003434.
Grandin, R., A. Socquet, C. Doubre, E. Jacques, and G. C. P. King (2012), Elastic thickness control of lateral dyke intrusion at mid-ocean ridges, *Earth Planet. Sci. Lett.*, *319–320*, 83–95.
Gualda, G. A. R., M. S. Ghiorso, R. V. Lemons, and T. L. Carley (2012), Rhyolite-MELTS: A modified calibration of MELTS optimized for silica-rich, fluid-bearing magmatic systems, *J. Petrol.*, *53*, 875–890.
Gudmundsson, M. T., et al. (2016), Gradual caldera collapse at Bárdarbunga volcano, Iceland, regulated by lateral magma outflow, *Science*, *353*, aaf8988, doi:10.1126/science.aaf8988.
Hildreth, W., and J. Fierstein (2000), Katmai volcanic cluster and the great eruption of 1912, *Geol. Soc. Am. Bull.*, *112*, 1594–1620.
Holmes, A., and H. F. Harwood (1929), The tholeiites of the north of England, *Miner. Mag.*, *22*, 1–52.
Ishizuka, O., R. N. Taylor, J. A. Milton, and R. W. Nesbitt (2003), Fluid-mantle interaction in an intra-oceanic arc: Constraints from high-precision Pb isotopes, *Earth Planet. Sci. Lett.*, *211*, 221–236.
Ishizuka, O., N. Geshi, J. Itoh, Y. Kawanabe, and T. Tuzino (2008), The magmatic plumbing of the submarine Hachijo NW volcanic chain, Hachijojima, Japan: Long distance magma transport?, *J. Geophys. Res.*, *113*, B08S08, doi:10.1029/2007JB005325.
Ishizuka, O., N. Geshi, Y. Kawanabe, I. Ogitsu, R. N. Taylor, T. Tuzino, I. Sakamoto, K. Arai, and S. Nakano (2014), Long-distance magma transport from arc volcanoes inferred from the submarine eruptive fissures offshore Izu-Oshima volcano, Izu-Bonin arc, *J. Volcanol. Geotherm. Res.*, *285*, 1–17.
Ishizuka, O., R. N. Taylor, N. Geshi, T. Oikawa, Y. Kawanabe, and I. Ogitsu (2015), Progressive mixed-magma recharging of Izu-Oshima volcano, Japan: A guide to magma chamber volume, *Earth Planet. Sci. Lett.*, *430*, 19–29.
Johnson, C. M., and B. L. Beard (1999), Correction of instrumentally produced mass fractionation during isotopic analysis of Fe by thermal ionization mass spectrometry, *Int. J. Mass Spectrom.*, *193*, 87–99.
Jolly, R. J. H., and D. J. Sanderson (1995), Variation in the form and distribution of dykes in the Mull swarm, Scotland, *J. Struct. Geol.*, *17*, 1543–1557.
Kent, R. W., and G. Fitton (2000), Mantle sources and melting dynamics in the British palaeogene igneous province, *J. Petrol.*, *41*, 1023–1040.
Kerr, A. C. (1993), The geochemistry and petrogenesis of the Mull and Morvern Tertiary lava succession, Argyll, Scotland, PhD thesis, Univ. of Durham, Durham, U. K.
Kerr, A. C. (1994), Lithospheric thinning during the evolution of continental large igneous provinces: A case study from the North Atlantic Tertiary Province, *Geology*, *22*, 1027–1030.
Kerr, A. C. (1995), The geochemistry of the Mull–Morvern Tertiary lava succession, NW Scotland: An assessment of mantle sources during plume related volcanism, *Chem. Geol.*, *122*, 43–58.
Kerr, A. C., P. D. Kempton, and R. N. Thompson (1995), Crustal assimilation during turbulent magma ascent (ATA); new isotopic evidence from the Mull Tertiary lava succession, NW Scotland, *Contrib. Mineral. Petrol.*, *119*, 142–154.
Kerr, A. C., R. W. Kent, B. A. Thomson, J. K. Seedhouse, and C. H. Donaldson (1999), Geochemical evolution of the Tertiary Mull volcano, western Scotland, *J. Petrol.*, *40*, 873–908.
Klein, E. M., and C. H. Langmuir (1987), Global correlations of ocean ridge basalt chemistry with axial depth and crustal thickness, *J. Geophys. Res.*, *92*, 8089–8115, doi:10.1029/JB092iB08p08089.
Klugel, A., M. A. Longpre, L. García-Cañada, and J. Stix (2015), Deep intrusions, lateral magma transport and related uplift at ocean island volcanoes, *Earth Planet. Sci. Lett.*, *431*, 140–149.
Lambert, R. S. J. (1958), A metamorphic boundary in the Moine schists of the Morar and Knoydart districts of Inverness-shire (northwest Scotland), *Geol. Mag.*, *95*, 177–194.
Lister, J. R., and R. C. Kerr (1991), Fluid-mechanical models of crack propagation and their application to magma-transport in dykes, *J. Geophys. Res.*, *96*, 10,049–10,077.
MacDonald, R., L. Wilson, R. S. Thorpe, and A. Martin (1988), Emplacement of the Cleveland Dyke: Evidence from geochemistry, mineralogy and physical modeling, *J. Petrol.*, *29*, 559–583.
MacDonald, R., B. Bagiński, B. G. J. Upton, P. Dzierżanowski, and W. Marshall-Roberts (2009), The Palaeogene Eskdalemuir dyke, Scotland: Long distance lateral transport of rhyolitic magma in a mixed magma intrusion, *Miner. Mag.*, *73*, 285–300.
MacDonald, R., B. Bagiński, B. G. J. Upton, H. Pinkerton, D. A. MacInnes, and J. C. MacGillivray (2010), The Mull Palaeogene dyke swarm: Insights into the evolution of the Mull igneous centre and dyke-emplacement mechanisms, *Miner. Mag.*, *74*, 601–622.
MacDonald, R., B. Bagiński, D. A. MacInnes, J. C. MacGillivray, and D. J. Fettes (2014), The Palaeogene Bracken Bay–Straiton dyke: Composition and controls on intrusion, *Scott. J. Geol.*, *50*, 57–69, doi:10.1144/sjg2013-009.
MacDonald, R., D. J. Fettes, and B. Bagiński (2015), The Mull Paleocene dykes: Some insights into the nature of major dyke swarms, *Scott. J. Geol.*, *51*, 116–124, doi:10.1144/sjg2014-016.
Magee, C. (2011), Emplacement of sub-volcanic cone sheet intrusions, PhD thesis, Univ. of Birmingham, Birmingham, U. K.
Magee, C., C. T. E. Stevenson, B. O'Driscoll, and M. S. Petronis (2012a), Local and regional controls on the lateral emplacement of the Ben Hiant Dolerite intrusion, Ardnamurchan (NW Scotland), *J. Struct. Geol.*, *39*, 66–82, doi:10.1016/j.jsg.2012.03.005.
Magee, C., C. Stevenson, B. O'Driscoll, N. Schofield, and K. McDermott (2012b), An alternative emplacement model for the classic Ardnamurchan cone sheet swarm, NW Scotland, involving lateral magma supply via regional dykes, *J. Struct. Geol.*, *43*, 73–91, doi:10.1016/j.jsg.2012.08.004.
Magee, C., et al. (2016), Lateral magma flow in mafic sill complexes, *Geosphere*, *12*, 809–841, doi:10.1130/GES01256.1.
Martí, J., V. Pinel, C. López, A. Geyer, R. Abella, M. Tárraga, M. J. Blanco, A. Castro, and C. Rodríguez (2013), Causes and mechanisms of the 2011–2012 El Hierro (Canary Islands) submarine eruption, *J. Geophys. Res. Solid Earth*, *118*, 823–839, doi:10.1002/jgrb.50087.

Meyer, R., G. R. Nicoll, J. Hertogen, V. R. Troll, R. M. Ellam, and C. H. Emeleus (2009), Trace element and isotope constraints on crustal anatexis by upwelling mantle melts in the North Atlantic Igneous Province: An example form the Isle of Rum, NW Scotland, *Geol. Mag.*, *146*, 382–399.
Morrison, M. A., R. N. Thompson, I. L. Gibson, and G. F. Marriner (1980), Lateral chemical heterogeneity in the Palaeocene upper mantle beneath the Scottish Hebrides, *Philos. Trans. R. Soc. London A*, *297*, 229–244.
Morrison, M. A., R. N. Thompson, and A. P. Dickin (1985), Geochemical evidence for complex magmatic plumbing during development of a continental volcanic center, *Geology*, *13*, 581–584.
Mussett, A. E. (1986), ^{40}Ar-^{39}Ar step-heating ages of the Tertiary igneous rocks of Mull, Scotland, *J. Geol. Soc. London*, *143*, 887–896.
Nakamura, K. (1977), Volcanoes as possible indicators of tectonic stress orientation-principle and proposal, *J. Volcanol. Geotherm. Res.*, *2*, 1–16.
Nishimura, T., S. Ozawa, M. Murakami, T. Sagiya, T. Tada, M. Kaizu, and M. Ukawa (2001), Crustal deformation caused by magma migration in the northern Izu Islands, Japan, *Geophys. Res. Lett.*, *28*, 3745–3748.
Owen, S., P. Segall, M. Lisowski, A. Miklius, M. Murray, M. Bevis, and J. Foster (2000), January 30, 1997 eruptive event on Kilauea Volcano, Hawaii, as monitored by continuous GPS, *Geophys. Res. Lett.*, *27*, 2757–2760, doi:10.1029/1999GL008454.
Pankhurst, R. J., J. N. Walsh, R. D. Beckinsale, and R. R. Skelhorn (1978), Isotopic and other geochemical evidence for the origin of the Loch Uisg granophyre, Isle of Mull, Scotland, *Earth Planet. Sci. Lett.*, *38*, 355–363.
Pedersen, R., and F. Sigmundsson (2006), Temporal development of the 1999 intrusive episode in the Eyjafjallajökull volcano, Iceland, derived from InSAR images, *Bull. Volcanol.*, *68*, 377–393.
Peltier, A., V. Ferrazzini, T. Staudacher, and P. Bachèlery (2005), Imaging the dynamics of dyke propagation prior to the 2000–2003 flank eruptions at Piton de La Fournaise, Réunion Island, *Geophys Res Lett.*, *32*, L22302, doi:10.1029/2005GL023720.
Peltier, A., V. Famin, P. Bachèlery, V. Cayol, Y. Fukushima, and T. Staudacher (2008), Cyclic magma storages and transfers at Piton de La Fournaise volcano (La Réunion hotspot) inferred from deformation and geochemical data, *Earth Planet. Sci. Lett.*, *270*, 180–188.
Philpotts, A. R., and D. E. Philpotts (2007), Upward and downward flow in a camptonite dike as recorded by deformed vesicules and the anisotropy of magnetic susceptibility (AMS), *J. Volcanol. Geotherm. Res.*, *161*, 81–94, doi:10.1016/j.jvolgeores.2006.11.006.
Pinel, V., and C. Jaupart (2004), Magma storage and horizontal dyke injection beneath a volcanic edifice, *Earth Planet. Sci. Lett.*, *221*, 245–262.
Poland, M., A. Miklius, T. Orr, A. Sutton, C. Thornber, and D. Wilson (2008), New episodes of volcanism at Kilauea Volcano, Hawaii, *Eos Trans. AGU*, *89*, 37–38, doi:10.1029/2008EO050001.
Poland, M. P., A. Miklius, and E. K. Montgomery-Brown (2014), Magma supply, storage, and transport at shield-stage Hawaiian volcanoes, in *Characteristics of Hawaiian Volcanoes*, edited by M. P. Poland, T. J. Takahashi, and C. M. Landowski, *U.S. Geol. Surv. Prof. Pap.*, 1801, 179–234.
Rollinson, H. G. (2012), Geochemical constraints on the composition of Archaean lower continental crust: Partial melting in the Lewisian granulites, *Earth Planet. Sci. Lett.*, *351–352*, 1–12.
Rubin, A. M. (1990), A comparison of rift-zone tectonics in Iceland and Hawaii, *Bull. Volcanol.*, *52*, 302–319, doi:10.1007/BF00304101.
Rubin, A. M., and D. D. Pollard (1987), Origins of blade-like dikes in volcanic rift zones, in *Volcanism in Hawaii*, edited by R. W. Decker, T. L. Wright, and P. H. Stauffer, *U.S. Geol. Surv. Prof. Pap.*, 1350, 1449–1470.
Rust, A. C., M. Manga, and K. V. Cashman (2003), Determining flow type, share rate and share stress in magmas from bubble shapes and orientations, *J. Volcanol. Geotherm. Res.*, *122*, 111–132.
Ryan, M. P. (1988), The mechanics and three-dimensional internal structure of active magmatic systems: Kilauea Volcano, Hawaii, *J. Geophys. Res.*, *93*, 4213–4248.
Saunders, A. D., J. G. Fitton, A. C. Kerr, M. J. Norry, and R. W. Kent (1997), The North Atlantic Igneous Province, in *Large Igneous Provinces: Continental, Oceanic and Planetary Volcanism*, edited by J. J. Mahoney and M. F. Coffin, *Geophys. Monogr., AGU*, 100, 45–93.
Sinton, J., E. Bergmanis, K. Rubin, R. Batiza, T. K. P. Gregg, K. Grönvold, K. C. Macdonald, and S. M. White (2002), Volcanic eruptions on mid-ocean ridges: New evidence from the superfast spreading East Pacific Rise, 17°–19°S, *J. Geophys. Res.*, *107*(B6), doi:10.1029/2000JB000090.
Skelhorn, R. R., J. D. S. MacDougall, and P. J. N. Longland (1969), The Tertiary igneous geology of the Isle of Mull, *Geol. Assoc. Guides*, *20*, 36 pp.
Smith, D. I., and J. Watson (1983), Scale and timing of movements on the Great Glen fault, Scotland, *Geology*, *11*, 523–526.
Speight, J. M., R. R. Skelhorn, T. Sloan, and R. J. Knapp (1982), The dyke swarms of Scotland, in *Igneous Rocks of the British Isles*, edited by D. S. Sutherland, pp. 449–459, John Wiley, Chichester, U. K.
Tanaka, T., et al. (2000), JNdi-1: A neodymium isotopic reference in consistency with LaJolla neodymium, *Chem. Geol.*, *168*, 279–281.
Taylor, R. N., O. Ishizuka, A. Michalik, J. A. Milton, and I. W. Croudace (2015), Evaluating the precision of Pb isotope measurement by mass spectrometry, *J. Anal. At. Spectrom.*, *30*, 198–213, doi:10.1039/C4JA00279B.
Thirlwall, M. E. (1991), Long-term reproducibility of multicollector Sr and Nd isotope ratio analysis, *Chem. Geol.*, *94*, 85–104.
Thirlwall, M. E., M. A. M. Gee, R. N. Taylor, and B. J. Murton (2004), Mantle components in Iceland and adjacent ridges investigated using double-spike Pb isotope ratios, *Geochim. Cosmochim. Acta*, *68*(2), 361–386.
Thompson, R. N., A. P. Dickin, I. L. Gibson, and M. A. Morrison (1982), Elemental fingerprints of isotopic contamination of Hebridean Palaeocene mantle-derived magmas by Archaean sial, *Contrib. Mineral. Petrol.*, *79*, 159–168.
Thompson, R. N., I. L. Gibson, and R. S. Harmon (1986), Two contrasting styles of interaction between basic magmas and continental crust in the British Tertiary Volcanic Province, *J. Geophys. Res.*, *91*, 5985–5997.
Thomson, B. A. (1986), The petrology and geochemistry of the Tertiary cone-sheet complex, Island of Mull, Scotland, PhD thesis, Univ. of London, London, U. K.
Toda, S., R. S. Stein, and T. Sagiya (2002), Evidence from the AD 2000 Izu islands earthquake swarm that stressing rate governs seismicity, *Nature*, *419*, 58–61.
Tryggvason, E. (1984), Widening of the Krafla fissure during the 1975–1981 volcanotectonic episode, *Bull. Volcanol.*, *47*, 47–69.
Tyrrell, G. W. (1917), Some Tertiary dykes of the Clyde area, *Geol. Mag.*, *4*, 305–315.
Walsh, J. N., R. D. Beckinsale, R. R. Skelhorn, and R. S. Thorpe (1979), Geochemistry and petrogenesis of Tertiary granitic rocks from the Island of Mull, Northwest Scotland, *Contrib. Mineral. Petrol.*, *71*, 99–116.
Watanabe, T., T. Koyaguchi, and T. Seno (1999), Tectonic stress controls on ascent and emplacement of magmas, *J. Volcanol. Geotherm. Res.*, *91*, 65–78.
White, R. S. (1988), A hot-spot model for early Tertiary volcanism in the North Atlantic, in *Early Tertiary Volcanism and the Opening of the NE Atlantic*, edited by A. C. Morton and L. M. Parson, *Geol. Soc., London, Spec. Publ.*, 39, 3–13.
Whitehouse, M. J. (1990), Isotopic evolution of the southern Outer Hebridean Lewisian gneiss complex: Constraints on Late Archaean source regions and the generation of transposed Pb-Pb palaeoisochrons, *Chem. Geol.*, *86*, 1–20.
Whitehouse, M. J., and C. J. Robertson, (1995), Isotopic evolution of the Lewisian Complex of Tiree, Inner Hebrides and correlation with the mainland, *Scott. J. Geol.*, *31*, 131–137.
Yamaoka, K., M. Kawamura, F. Kimata, N. Fujii, and T. Kudo, (2005), Dike intrusion associated with the 2000 eruption of Miyakejima Volcano, Japan, *Bull. Volcanol.*, *67*, 231–242.